Annales Societatis Geologorum Poloniae (2026), vol. 96: ...–... https://doi.org/10.14241/asgp.2026.03

DIAGENESIS OF SILICEOUS SPONGE SPICULES: MICROSTRUCTURAL AND MINERALOGICAL MODIFICATIONS OF BIOSILICA WITH TIME

Andrzej PISERA[1*], **Sylvie MASSE**[2], **Mohamed SELMANE**[3] **& Magdalena ŁUKOWIAK**[1]

[1] *Institute of Paleobiology, Polish Academy of Sciences, Twarda 51/55, 00-818 Warszawa, Poland; e-mails: apis@twarda.pan.pl, mlukowiak@twarda.pan.pl*
[2] *Sorbonne Université, CNRS, Laboratoire de Chimie de la Matière Condensée de Paris, LCMCP, F-75005, Paris, France; sylvie.masse@sorbonne-universite.fr*
[3] *Sorbonne Université, CNRS, Fédération de Chimie et Matériaux de Paris-Centre, FCMat, F-75005, Paris, France; e-mail: mohamed.selmane@sorbonne-universite.fr*
** Corresponding author*

Pisera, A., Masse, S., Selmane, M. & Łukowiak, M., 2026. Diagenesis of siliceous sponge spicules: microstructural and mineralogical modifications of biosilica with time. *Annales Societatis Geologorum Poloniae*, 96: xx–xx.

Abstract: The diagenesis of biosilica remains poorly known, but is increasingly important for reconstructing past oceanic silica levels using silicon isotopes. Here, we present SEM and XRD analyses of sponge spicules from the Late Jurassic, Late Cretaceous, and Eocene, compared with modern samples, to reveal their modifications with time. Modern spicules are composed of opal-A, distinct from sinter-derived opal-A. Many Eocene spicules also preserve opal-A, but show signs of early transformation. Most Eocene and all Cretaceous spicules consist of opal-CT, while quartz occurs in some Cretaceous and all Jurassic samples. Eocene opal-A spicules are macroscopically glassy, whereas opal-CT spicules exhibit a milky and/or opaque appearance, due to the presence of silica microspheres. Cretaceous spicules range from milky to opaque, and Jurassic spicules are typically opaque, containing microspheres, silica nanogranules, and microquartz. The structural and mineralogical evolution is reflected in decreasing Full Width at Half Maximum (FWHM) values of diffractograms with increasing age. Some Cretaceous and Jurassic spicules contain quartz blocks, formed by the fusion of silica nanogranules, while euhedral quartz occurs in both Cretaceous and Jurassic samples. Although diagenetic stages can vary within a single spicule, all retain at least some elements of their original structure and morphology. The observed mineralogical transitions reflect dominant solid-state maturation through dehydration and sintering and/or Ostwald ripening, rather than dissolution, mould formation, and reprecipitation from external fluids. Our findings indicate that sponge spicules preserved through solid-state transformation are preferred targets for silicon isotope studies. However, the assumption that such spicules retain their original isotopic signal must be further verified through integrated structural and isotopic investigations.

Key words: Sponge spicules, Recent, fossil, opal-A, opal-CT, quartz, solid-state transformation.

Manuscript received 16 November 2025, accepted 5 May 2026

INTRODUCTION

Although silica diagenesis has been widely studied (e.g., Calvert, 1974; Wise and Weaver, 1974; Kastner *et al*., 1977; Williams and Crerar, 1985; Williams *et al.*, 1985; Hesse, 1989; Lynne and Campbell, 2003, 2004; Lynne *et al.*, 2005, 2007, 2008) and is generally understood to follow a path from amorphous opal-A, through opal-CT, to quartz (Demaster, 2005), some of its details remain poorly understood. In particular, the diagenesis of biosilica, such as sponge spicules, which are common in sedimentary rocks, has received limited attention. Exceptions include studies on Eocene (Frisone *et al.*, 2014), Cretaceous and Permian spiculites (e.g., Matysik *et al.*, 2018; Jurkowska *et al.*, 2026), which mainly focus on host-rock petrography and adopt a "dissolution–mould formation–mould infilling" model of spicule diagenesis. Recently, Stamm *et al.* (2025) presented a comparative analysis of the geochemical and mineralogical composition, as well as the isotopic signatures, of Recent and Cretaceous sponge spicules exhibiting various types of preservation. They proposed a model of *"recrystallization of opal-A to opal-CT induced by a dissolution-reprecipitation process during diagenesis"* to explain the modifications observed in fossil

spicules, although no accompanying structural analyses were conducted.

Understanding spicule diagenesis requires first considering the structure of modern spicules. Contrary to the simplistic view of spicules as rods of amorphous silica (essentially silica glass – see, for example, Matysik *et al*., 2018; Slagter *et al*., 2025; Stamm *et al.,* 2025), they are, in fact, complex biocomposites, made of silica and organic components – including proteins like collagen – and exhibit a complex internal structure (e.g., Schwab and Shore, 1971; Uriz *et al.*, 2000, 2003; Pisera, 2003; Weaver and Morse, 2003; Weaver *et al.*, 2003; Uriz, 2006; Woesz *et al.*, 2006; Schröder *et al.*, 2007; Ehrlich *et al.*, 2008, 2010; Müller *et al.*, 2008; Görlich *et al.*, 2020; Pisera *et al*., 2021, among others).

The spicule structure varies between Demospongiae and Hexactinellida – the two sponge classes with siliceous spicules, commonly preserved in the fossil record. Furthermore, lithistid demosponges differ from typical demosponges in having articulated spicules called desmas (Pisera, 2003). Spicules generally form around an organic axial filament (Pisera, 2003; Uriz *et al.*, 2003; Weaver and Morse, 2003; Uriz, 2006), long thought to consist of silicatein – an enzyme, believed to catalyse biosilica formation in sponges (Müller *et al.*, 2007). However, it is now known that the filament is primarily composed of actin, a highly abundant structural protein (Ehrlich *et al.*, 2022; Voronkina *et al.*, 2025). After the removal of the axial filament, a narrow axial canal typically remains, usually less than 1 μm in diameter (Uriz *et al*., 2000; Pisera, 2003; Weaver and Morse, 2003; Weaver *et al.*, 2003). Some lithistid spicules lack an axial filament but still show a concentration of organic material at the centre (Pisera, 2003).

The diagenesis of siliceous spicules has become a critical issue, due to the increasing use of silicon isotopes in reconstructing past oceanic silica levels (e.g., De La Rocha, 2003; Hendry *et al.*, 2010; Wille *et al.*, 2010; Hendry and Robinson, 2012; Fontorbe *et al.*, 2016, 2017; Frings *et al*., 2016; Łukowiak, 2020; Stamm *et al.*, 2025). These silica levels are closely linked to the carbon cycle (Tréguer *et al.*, 2021), which, in turn, plays a key role in regulating climate. Consequently, palaeoclimate reconstructions, based on the silicon isotopic composition of biosilica, must assess whether fossil siliceous spicules preserve their original isotopic signatures (cf. Slagter *et al*., 2025; Stamm *et al*., 2025), whether they have undergone diagenetic alteration, and, if so, the nature of such modifications.

The objective of this study is to examine and elucidate the modification of biosilica in spicules with geological time, thereby contributing to a broader understanding of silica diagenesis in sedimentary environments, including isotopic studies, and providing insights into the interpretation of diagenetic sequences in spiculitic rocks.

MATERIAL

We examined fossil spicules from the Eocene, Upper and Lower Cretaceous, and Upper Jurassic deposits. All are macroscopically well-preserved, retaining sculptural details, such as tubercles and spines. For comparison, we also examined siliceous spicules from extant sponges.

Recent spicules

The spicules of major siliceous sponge groups that preserve in the fossil record were studied (for the classification of sponges, see Hooper and Van Soest, 2002) including 1) Hexactinosan sponges, such as *Laocoetis* and *Aphrocallistes* (Hexactinellida, Hexactinosida) with a fused skeleton; 2) lithistid demosponges (Demospongiae) with an articulated desma skeleton, including: megaclones of *Pleroma,* dicranoclones of *Corallistes*, and various *rhizoclones*; and 3) "soft" demosponges (Demospongiae), such as strongyles of *Petrosia*. All these sponges originate mostly from deep waters of either the New Caledonia region or Madagascar.

Eocene spicules

Southern Ukraine. The spicules were collected from two locations:

Rybalski Quarry – Obukhov Formation, composed of dark grayish-green and brown silty sands and clays, often glauconitic and rich in siliceous spicules and fragments of lithistid sponges and the borehole no. 143 – from green-grey glauconitic sands of the Southwestern Australia (for details, see Łukowiak *et al*., 2022a). The spicules were collected from Upper Eocene spiculites and spongiolites of the Pallinup Formation, at Fitzgerald River National Park and Doyle Road, east of Hopetoun (for details, see Gammon *et al*., 2000; Gammon and James, 2003; Łukowiak, 2015, 2016; Łukowiak and Pisera, 2017; Pisera *et al*., 2023). In both cases, lithistid desmas as well as oxeas and triaenes of soft demosponges (Demospongiae, Astrophorida) were studied.

Cretaceous spicules

These spicules come from Misburg, Oberg, and Höver (Northern Germany) and were recovered from Upper Cretaceous (Campanian) marls, previously referred to as "Quadraten-Kreide" and "Mucronaten-Kreide" (Schrammen, 1910–1912; Wiese *et al*., 2013). Both fused hexactinellid skeletons (*Aphrocallistes*) and undetermined lychniscosan sponges (Hexactinellida, Lychniscosida), along with megaclone, dicranoclone, and tetraclone desmas of undetermined lithistids, as well as astrophorid triaenes (Demospongiae, Astrophorida), were studied.

Additionally, Lower Cretaceous hexactinellid spicules from northern Spain were examined. These represent the only spicules studied that come from limestones tectonically involved in the Spanish Pyrenees (Lagneau-Hérenger, 1962).

Jurassic spicules

The samples were collected from the following locations: 1) Trzebinia (Poland) – Sponge Marly Limestones, Middle Oxfordian, Transversarium Zone (Trammer, 1989); 2) Zalas (Poland) – Jasna Góra Beds, marls and limestones

of the Middle Oxfordian, Plicatilis Zone (see Matyja and Tarkowski, 1981; Trammer, 1982; Matyja, 2006; Matyja *et al.*, 2006); 3) Wrzosowa (Poland) – Jasna Góra Beds, limestones and marls of the Lower Oxfordian, Cordatum Zone (Trammer, 1982; Matyja *et al.*, 2006).

The studied samples primarily contain rhizoclone desmas and hexactinellid spicules (*Laocoetis* and other undetermined hexactinosids), with admixtures of "soft" demosponge spicules in some cases. Additionally, diagenetic silica embedding rhizoclone desmas was studied.

METHODS

Spicules of extant sponges were cleaned of organic matter by heating sponge fragments in hot nitric acid until no further reaction was observed. The fossil spicules were extracted from the host rock using different methods, depending on the lithology. For the Late Jurassic and Early Cretaceous limestones, as well as the Late Cretaceous marls, the calcareous matrix was dissolved using either acetic acid or hydrochloric acid. In contrast, the Eocene samples, composed of soft sediments, required only simple washing. The spicules were then manually picked under a binocular microscope and classified, on the basis of their external appearance (translucent, opaque, or white) and systematic position.

The structural details of silica in the spicules, including surface features and broken transverse sections, were analyzed using a scanning electron microscope (SEM), while their mineral composition was determined via X-ray diffraction (XRD). FWHM (full width at half maximum) values of diffractograms were used in the interpretation of the various mineralogical phases of silica (Herdianita *et al.*, 2000a, b).

The mineralogical composition of spicules was then correlated with structural features. To examine the internal structures in greater detail, opaque and white spicules from the Eocene of Australia were etched in NaOH for 48 hours to expose the internal features.

Samples prepared for SEM structural observations were sputter-coated with platinum and examined at 25 kV, using a Philips XL-20 scanning electron microscope at the Institute of Paleobiology in Warsaw. Over 260 SEM photos were analysed.

XRD analyses of 43 samples were performed using a powder diffractometer, X'Pert PRO MPD (PANalytical B.V., Netherlands), with the DSH method at the Laboratory of Electron Microscopy, Microanalysis, and X-ray Diffraction, Faculty of Geology, University of Warsaw. The measurements were conducted in the 2θ range of 6–90° with a step size of 0.026°. Powder samples were sealed in capillaries, made of non-reflecting glass with an inner diameter of 0.5 mm. CoKα radiation was used, with operational parameters of 35 mA and 40 kV. Data acquisition was carried out with a fast linear PIXcel detector, and the total measurement time per sample was six hours. XRD data processing was performed using WinPLOTR (Roisnel *et al*., 2001) or Fullprof suite software.

The terminology, classification, and interpretation of silica phases follow the studies of siliceous sinters and other sedimentary siliceous deposits (Jones and Segnit, 1971; Flörke *et al.*, 1991; Elzea *et al.*, 1994; Graetsch, 1994; Guthrie *et al.*, 1995; Elzea and Rice, 1996; Herdianita *et al.*, 2000a, b; Ilieva *et al*., 2007; Lee, 2007; Ghisoli *et al.*, 2010; Wilson, 2014; Frölich, 2020). Additionally, interpretations are based on research on siliceous sinters diagenesis (Lynne and Campbell, 2003, 2004; Rodgers *et al.*, 2004; Lynne *et al.*, 2005, 2007; Jones and Renaul, 2007; Jones, 2021), as well as studies of common and precious opals (Liesegang and Milke, 2014 and Liesegang *et al.*, 2018).

AN INTRODUCTION TO THE STRUCTURE AND MINERALOGY OF RECENT SPONGE SPICULES

Recent sponge spicules typically show a layered structure (Fig. 1C–H), made of silica nanogranules (Fig. 1C–E, I; Pisera, 2003; Uriz *et al*., 2003; Woesch *et al*., 2006) that is well visible after nitric acid treatment that oxidizes organics. Nanogranule size varies among sponges and even within individual spicules (Pisera, 2003; Fig. 1D). Spicule structures differ in hexactinellids (Fig. 1G, H), demosponges (Fig. 1C, F), and lithistids (Fig. 1D, E), potentially affecting diagenesis (Pisera, 2003; Weaver *et al*., 2003; Woesch *et al*., 2006; Pisera *et al*., 2021). Hexactinellid spicules show more regular layering, with distinct, separable layers (Sandford, 2003; Woesch *et al*., 2006; Fig. 1G, H). In contrast, regular demosponge spicules lack clear layers, displaying instead a concentric arrangement of nanospheres and larger granules (Fig. 1). Lithistid spicules also exhibit concentric structures, though often irregular (Fig. 1D, E), with smaller, denser granules in the outer layers and larger or hollow ones toward the central part. This pattern suggests different silica depositional processes (Fig. 1D; Pisera, 2003; Pisera *et al*., 2021; Shimizu *et al*., 2024).

An axial canal, resulting from the removal of the organic axial filament, can be observed in the central region of the spicules (Fig. 1A–C), except in some lithistids. The canal shape varies from triangular in typical demosponges (Fig. 1B, C) to square in hexactinellids (not shown). Regardless of their taxonomic position – whether lithistid desmas, other demosponge spicules, or hexactinosan skeletons – these specimens remain glassy and translucent, even after decades in collections.

X-ray diffraction of spicules reveals broad peaks near 25.54–25.82° 2Θ (Fig. 2; Tab. 1), indicating poorly crystalline silica, typical of opal-A (Jones and Segnit, 1971; Elzea *et al.*, 1994; Herdianita *et al*., 2000a, b; Lynne *et al*., 2005, 2007, 2008; Lee, 2007; Liesegang *et al*., 2018).

RESULTS

Eocene spicules from SW Australia

Only demosponge spicules – both lithistid and non-lithistid – were available for the study. They are glassy, opaque, and milky, with some spicules showing both translucent and opaque/white regions.

Table 1

Mineralogy of Recent and fossil sponge spicules, as revealed by X-ray analysis (taxonomy and terminology of spicules after Hooper and Van Soest, 2002 and Łukowiak *et al.,* 2022b).

No.	Description	Pos. [°2Th.]	FWHM [°2Th.]	d-spacing [A]	Mineralogy
18-11	Recent (SW Pacific), dicranoclone lithistid desmas (Demospongiae)	25.66	7.84	4.028	Opal-A
18-13	Recent (Indian Ocean), fused skeleton of *Laocoetis* (Hexactinellida)	25.81	7.78	4.005	Opal-A
18-16	Recent (SW Pacific), petrosid demosponge (Demspongiae)	25.77	7.67	4.011	Opal-A
18-15	Recent, fused skeleton of *Aphrocallistes* (Hexactinellida)	25.77	7.57	4.012	Opal-A
18-12	Recent (Indian Ocean), *Laocoetis* fused skeleton (Hexactinellida)	25.78	7.48	4.009	Opal-A
18-14	Recent, rhizoclone desmas (Demospongiae)	25.54	7.40	4.047	Opal-A
ST-10	Recent, Indonesia, *Tedania* (Demospongiae)	25.82	7.35	4.003	Opal-A
ST-66	Eocene, Ukraine, triaenes (Demospongiae), glassy	25.37	7.09	4.074	Opal-A
ST-67	Ukraine, triaenes (Demospongiae), glassy	25.43	6.89	4.064	Opal-A
ST-86	Eocene, Ukraine, various spicules (Demospongiae), glassy	25.35	6.88	4.076	Opal-A
ST-58	Eocene, Australia, megaclone desmas (Demospongiae), glassy	25.47	6.93	4.058	Opal-A
ST-62	Eocene, Australia, rhizoclone desmas (Demospongiae), glassy	24.98	6.40	4.135	Opal-A/CT?
18-08	Eocene, Australia, various spicules, (Demospongiae), glassy	25.34	6.35	4.078	Opal-A
18-17	Eocene, Australia, lithistid desmas (Demospongiae), glassy	25.16	5.54	4.107	Opal-A/CT?
ST-60	Eocene, Australia, megaclone desmas (Demospongiae), milky to opaque	24.85	1.58	4.157	Opal-CT
ST-63	Eocene, Australia, megaclone desmas (Demospongiae), milky/opaque	24.91	1.24	4.147	Opal-CT
ST-71	Eocene, Australia triaenes (Demospongiae), opaque	24.93	1.34	4.145	Opal-CT
St-50	Eocene, Australia, megaclone desmas (Demospongiae), opaque	24.88	1.19	4.152	Opal-CT
ST-52	Eocene, Australia, megaclone desmas (Demospongiae), white iridescent	24.82	7.11	4.162	Opal-A/CT
ST-64	Eocene, Australia, megaclone desmas (Demospongiae), white iridescent	24.94	6.70	4.143	Opal-A/CT
ST-57	Cretaceous, Germany, dicranoclone desmas (Demospongiae)	25.17	1.02	4.105	Opal-CT
ST-101	Cretaceous, Germany, megaclone desmas (Demospongiae)	24.99	1.09	4.135	Opal-CT
18-05	Cretaceous, Germany, calthrops (Demospongiae)	25.04	0.95	4.126	Opal CT
18-04	Cretaceous, Germany, *Aphrocallistes* fused skeleton (Hexactinellida)	23.99 25.03 30.80	0.76 0.74 0.28	4.303 4.128 3.368	Opal-CT Quartz
21-06	Cretaceous, Germany, lychniscosan fused skeleton (Hexactinellida)	24.23 25.25 31.03	0.26 0.87 0.18	4.263 4.092 3.35	Quartz Opal-CT Quartz

No.	Description	Pos. [°2Th.]	FWHM [°2Th.]	d-spacing [A]	Mineralogy
18-02	Jurassic, Poland (Zalas) rhizoclone lithistid desmas (Demospongiae)	25.14 23.90 30.81	0.95 0.71 0.27	4.110 4.320 3.368	Opal-CT Quartz
21-03	Jurassic, Poland (Zalas) hexactinosan fused skeleton (Hexactinellida)	24.22 25.23 31.00	0.57 0.80 0.16	4.264 4.095 3.347	Opal-CT Quartz
18-03	Jurassic, Poland (Trzebinia), *Laocoetis* fused skeleton (Hexactinellida)	24.14 30.81	0.18 0.26	4.278 3.368	Quartz Quartz
ZA-4	Jurassic, Poland (Zalas), diagenetic silica (precipitate)	24.06 30.84	0.19 0.23	4.292 3.364	Quartz Quartz

Translucent non-lithistid spicules have smooth surfaces with rare conchoidal etchings. At low magnification, cross-sections appear structureless, though concentric layering is visible (Fig. 3A, B). The axial canal is round and well visible (Fig. 3A), occasionally slightly triangular (Fig. 3B) in non-lithistids.

Opaque non-lithistid spicules show a rough surface due to their silica nanogranules. Cross-sections exhibit 5–10 μm microspheres, made of ~100 nm nanogranules and rods, embedded in the surrounding nanogranular matrix (70–150 nm in size; Fig. 3C–E). White non-lithistid spicules show a nanogranular structure of the outer layer (with some remnants of amorphous, smooth (glassy) silica; Fig. 3G), with silica microspheres protruding through (intersecting with) the surface (Fig. 3G–I) from the inside.

The white (milky) desma spicules of a lithistid *Pleroma* exhibit varying degrees of diagenetic alteration. Some of them have smooth surfaces with fissures. Fractured sections show an outer dense silica layer and an interior filled with 5–6 μm microspheres, separated from the matrix by small gaps (Fig. 4AC). Microspheres consist of 50–100 nm nanogranules (Fig. 4D) that cluster together. The matrix is also nanogranular (~100 nm), forming clusters interspersed with evenly distributed 30–40 nm nanopores (Fig. 4E, F). No original structures, including the axial canal, remain in these spicules, but *Pleroma* spicules lack an axial canal originally. In some cases, a sharp boundary divides translucent and milky regions within a spicule.

Cloudy or opaque *Pleroma* spicules exhibit rough surfaces, due to nanogranules (90–150 nm) and their aggregates. Some microspheres protrude through holes in the outer surface of the spicules (Fig. 5A, B). These are made of nanogranules of similar size (Fig. 5B). Fractured sections reveal irregularly clustered 4–15 μm microspheres within silica nanogranules (Fig. 5C, E, F). These contain well-defined, spherical or slightly elongated nanogranules (100–200 nm; Fig. 5G–I). No original internal structures are preserved.

White/milky spicules of *Pleroma* were also studied after etching in NaOH to reveal their silica structure. They show a dense, smooth, slightly cracked outer layer and a core of 2–10 μm microspheres (Fig. 6A, B). The outer crust, up to 6 μm thick, has round surface holes (~5 μm) that reveal internal microspheres (Fig. 6B, C). At low magnification, the surface appears smooth (Fig. 6B), but closer inspection reveals shallow, rounded etchings (Fig. 6C, D). The outer layer consists of coalescing ~50 nm nanogranules with similarly sized dispersed holes (Fig. 6D), and cross-sections show nanogranular layering (Fig. 6K, L).

Between microspheres, matrix remnants (removed by NaOH) contain 50–100 nm nanogranules (Fig. 6E, J). Larger microspheres have a porous outer crust of irregularly aligned nanogranules, forming contorted lamellae (Fig. 6E–H); their interiors are solid amorphous silica with few cracks (Fig. 6F, H, I). Smaller microspheres exhibit a spongy structure, made entirely of contorted lamellae of aligned nanogranules (Fig. 6G).

White iridescent spicules, all from a single specimen of *Pleroma*, differ from typical white spicules in displaying a dense network of surface fissures (Fig. 7A, B). Aside from these V-shaped, deep fissures, their surfaces remain smooth. The outer layer comprises irregular silica units, composed of coalescing nanogranules, 0.3–2 μm in diameter (Fig. 7C). Naturally broken cross-sections of these spicules reveal a porous core and a solid outer crust (~5–6 μm thick), with fissures confined to the crust (Fig. 7D). The crust is characterised by a clear nanogranular structure (~100 nm granules) and a well-defined boundary with the core, separated by a narrow transitional zone with sparse pores (Fig. 7E, F). Beneath the outer layer, the highly porous (foamy) core contains irregular pores, mostly 0.2–0.4 μm in diameter, with some up to 2–3 μm (Fig. 7G–I). The outer layer shows irregular, discontinuous layering (Fig. 7G), while the core silica is completely amorphous (Fig. 7I).

XRD analysis of noniridescent spicules produced diffractograms (samples 18-08, ST-58; Fig. 8), showing broad bands centred at 25.34–25.47° 2Θ (Fig. 8; Tab. 1), with FWHM and d-spacing values, characteristic of opal-A (Tab. 1). Others (e.g., ST-71, ST-50, ST-63, ST-60) show sharper, broad peaks

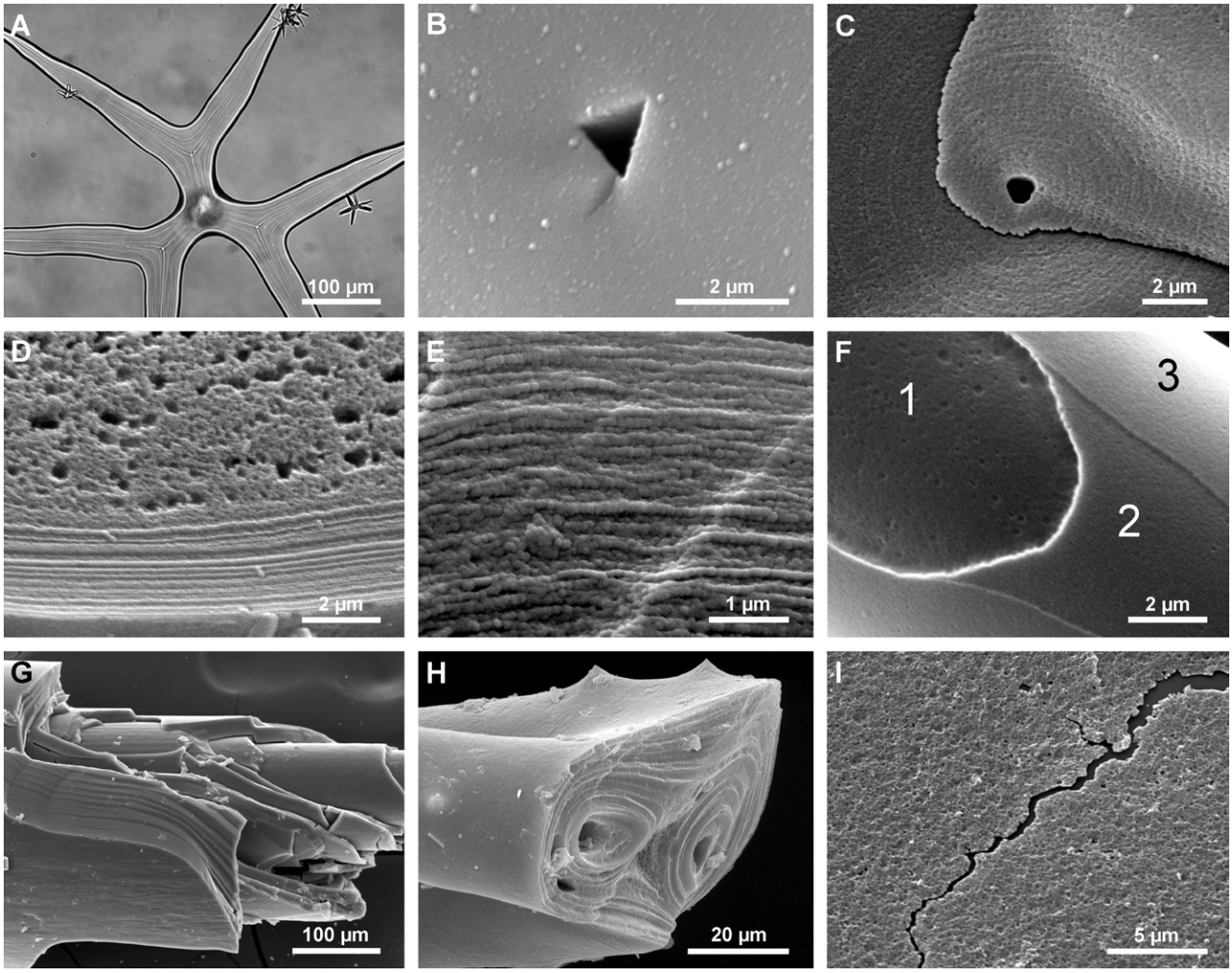

Fig. 1. Structure of extant sponge spicules. **A.** The axial canal of the lithistid demosponge ectosomal spicule is clearly visible within the spicule's arms. The canal extends along the entire length of the arm, with evident silica layering (transmitted light). **B.** Triangular axial canal of a non-lithistid demosponge spicule; natural broken surface. **C.** Cross-section of a demosponge spicule, showing a triangular axial canal and faint concentric layering, composed of silica nanogranules; natural broken surface. **D.** Different structural zones in a choanosomal desma spicule: a dense outer zone and a more porous inner zone. The outer part consists of regular layers of silica nanogranules; broken surface after treatment with nitric acid. **E.** Close-up of irregular layers in a desma spicule, composed of silica nanogranules; broken surface after treatment with nitric acid. **F.** Surface of a growing demosponge spicule, showing superimposed layers (marked with 1, 2, 3) that vary in silica sphere size and porosity – larger spheres and higher porosity in the inner layer, smaller spheres and lower porosity in the outer layer. **G.** Broken basal spicule of *Hyalonema* (Hexactinellida), displaying well-developed layering. **H.** Etched cross-section of *Aphrocallistes* (Hexactinellida), revealing a fused dictyonal skeleton with enlarged axial canals and distinct concentric layering. **I.** NaOH-etched fragment of the basal spicule of *Monorhaphis* (Hexactinellida), highlighting its granular nanostructure.

with a shoulder toward the lower angles, narrow FWHM, and d-spacing consistent with opal-CT (Elzea *et al*., 1994; Rodgers *et al*., 2004; Lynne *et al*., 2005, 2007, 2008; Wilson, 2014; Liesegang *et al*., 2018). A minor peak at ~41.5°2Θ (2.5247 Å) also indicates opal-CT. Some diffractograms (e.g., ST–62) display broad bands with distinct peaks – high FWHM (opal-A), but d-spacing closer to opal-CT – indicating opal-A/CT mixtures. Sharp quartz peaks (~31°2Θ) in some samples are attributed to contamination.

XRD diffractograms of fissured iridescent spicules display broad peaks, indicative of opal-CT, but with FWHM values closer to opal-A (Fig. 9; Tab. 1).

Eocene spicules from Ukraine

Only demosponge spicules, both lithistid and non-lithistid, were available for the study. Two types of preservation were identified: glassy and milky (white), with some spicules showing both translucent and white regions.

Translucent (glassy) spicules frequently have surfaces densely covered with shallow conchoidal depressions (a few micrometres wide). Fractured sections reveal a round axial canal, up to 30 µm in diameter (Fig. 10A), and concentric layering at lower magnifications (Fig. 10C); at higher magnifications, the silica is dense and consists of coalescing nanogranules (50–70 nm; Fig. 10B).

The surface of white (milky) spicules ranges from nearly smooth (Fig. 10E) to rough due to a granular structure (Fig. 10F, G) and is composed of coalescing nanogranules of various sizes. Microspheres from the interior intersect with this surface. The interior may consist of structureless (smooth) silica (likely corresponding to opal-A), interspersed with silica microspheres (Fig. 10D, E), or more commonly, it exhibits a nanogranular matrix with granules measuring ~100–200 nm, containing dispersed silica microspheres (Fig. 10H, I) and remnants of structureless (smooth) silica (Fig. 10I). Traces of original layering (Fig. 10D, E) and an enlarged, round axial canal are usually present (Fig. 10H).

Microspheres vary in size from 5 to 12 μm and consist of nearly structureless silica (Fig. 10F, I) or nanorods finer than the surrounding matrix (Fig. 10F).

XRD analysis, limited to translucent spicules due to the scarcity of other types of preservation, showed broad diffractograms centred at 25.35–25.43°2Θ (Fig. 11; Tab. 1),

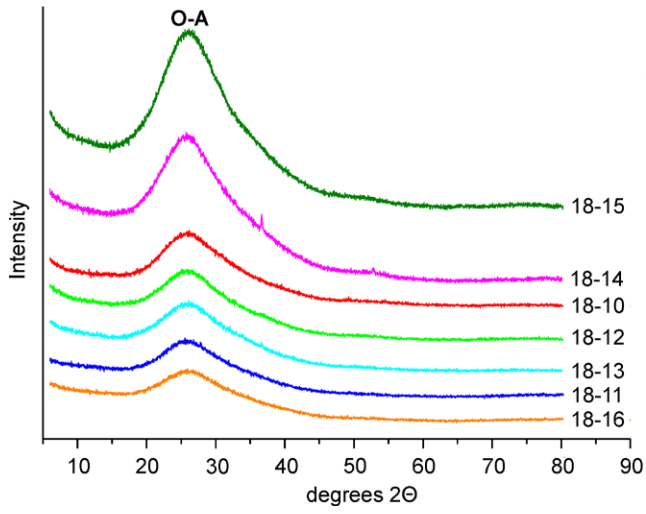

Fig. 2. Typical selected X-ray diffractograms of Recent spicules from different extant sponge groups (for sample characteristic see Table 1). O-A opal-A.

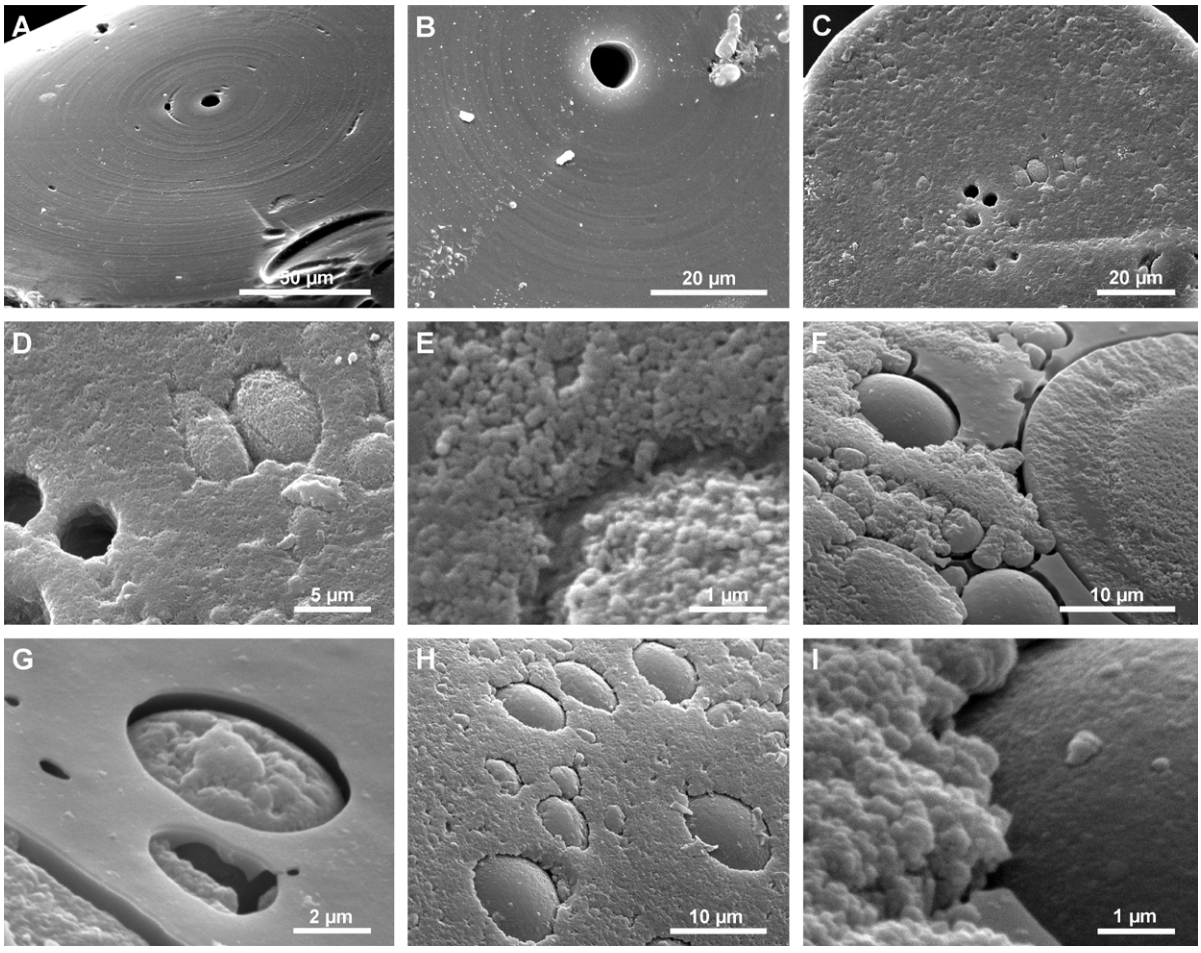

Fig. 3. Eocene nonlithistid demosponge spicules from SW Australia. **A, B.** Well-preserved translucent spicule, showing original layering and preserved axial canal (already enlarged and rounded, but with traces of original triangularity). **C, D.** General view of broken section of opaque spicule with preserved axial canals and showing microspheres of silica in matrix, composed of nanogranules. **E.** Enlargement of (D) showing details of matrix, composed of nanogranules and microsphere (right corner), also composed of nanogranules. **F, G.** Milky/white spicules; details of spicule surface, showing nanogranular matrix and microspheres with remnants of smooth (glassy) silica and intersection of microspheres formed inside the spicule with its surface; note that microspheres formed inside are composed of almost smooth silica. **H, I.** Spicule surface, showing nanogranular structure of outer layer intersecting with silica microspheres from inside the spicule: (I) magnification of (H), showing the contact between the outer layer (left), composed of nanogranules, and the surface of the microspheres from inside the spicule (right); note that the microspheres are nearly smooth.

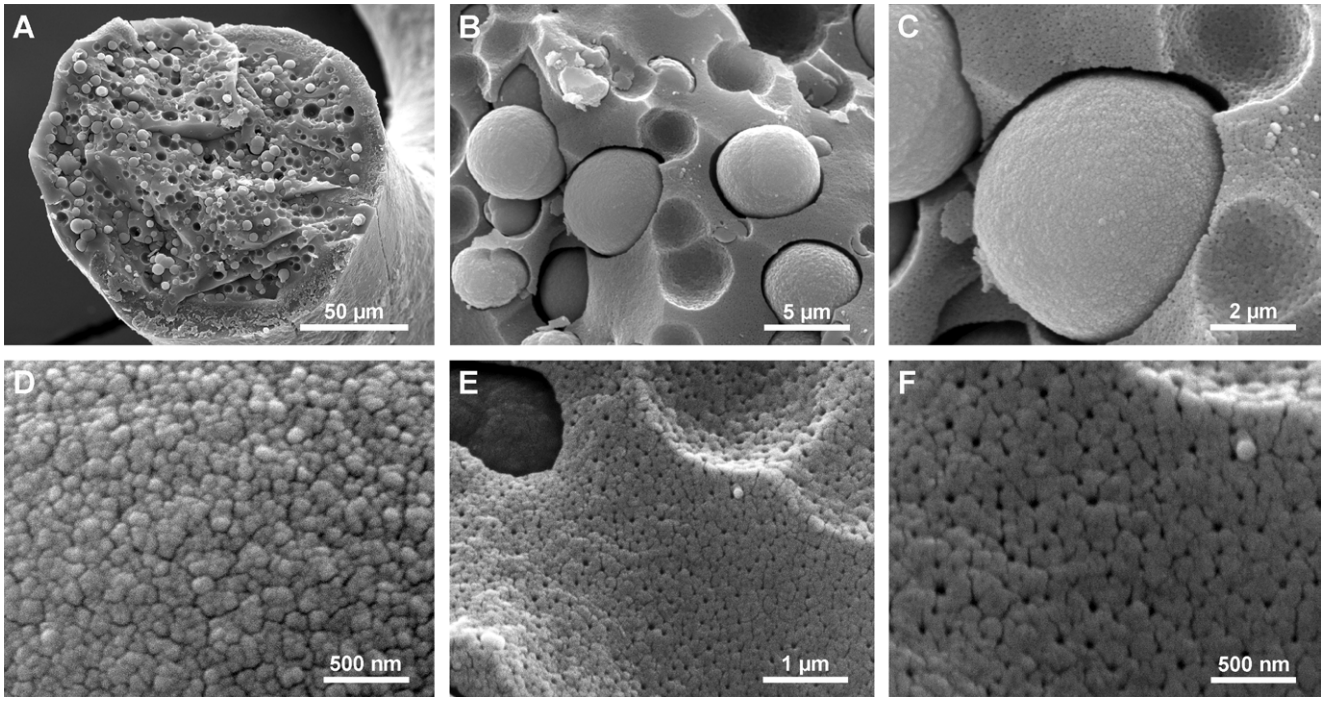

Fig. 4. Milky/white spicule of lithistid sponge *Pleroma*, Eocene, SW Australia. **A.** Broken cross-section, showing the absence of primary structures (e.g., axial canal or layering) and the presence of numerous silica microspheres. **B, C.** Close-up views of (A), highlighting microspheres embedded in the nanogranular matrix; note the consistent presence of a narrow space between the spheres and the surrounding matrix. **D.** Enlarged view of a microsphere's surface, revealing its composition of nanogranules. **E, F.** Details of the nanogranular matrix, with (F), showing numerous nanopores.

with FWHM and d-spacing typical of opal-A. A sharp peak at ~31°2Θ was also present, attributed to quartz contamination.

Late Cretaceous spicules

All Late Cretaceous spicules from Germany are opaque or white, lacking internal structures, except for the axial canal. Under transmitted light, spherical silica bodies are visible inside. Spicule surfaces are smooth or, more frequently, show angular depressions (Fig. 12A, H); where preserved, surfaces are smooth or covered with criss-crossing silica blades of aligned nanogranules (Fig. 12B, G, H) resembling, but less ordered than the opal-CT in lepispheres. Depressions expose clusters of nanogranules (50–100 nm; Fig. 12I).

A rim (0.7–1 µm thick) of criss-crossed bladed silica, composed of aligned nanogranules (100–150 nm), lines the axial canal (Fig. 12C, D). Cross-sections of other spicules reveal irregular silica blocks (1–2 µm), formed by coalescing nanogranules (~50–100 nm; Fig. 12D–F).

Some non-lithistid Late Cretaceous demosponge spicules have smooth surfaces with nanogranules and clusters (Fig. 13A, B); round holes expose well-developed internal lepispheres (2–5 µm; Fig. 13A, C). Lithistid (*Pleroma*) spicules differ, featuring a smooth outer nanogranular layer (50–100 nm; Fig. 13G, H) and internal microspheres (incipient lepispheres?) with aligned nanogranules, but no clear lamellae (Fig. 13H). Fractured surfaces reveal microspheres (up to 10 µm), made of embedded nanogranules (Fig. 13K, L).

Most X-ray diffractograms of the Late Cretaceous spicules show broad, strong peaks (24.99°–25.17° 2θ) with narrow FWHM and d-spacing values (Fig. 14; Tab. 1), typical of opal-CT, and a smaller opal-CT peak at ~42° 2θ. Some samples also show a minor quartz peak at ~31° 2θ.

One sample (no. 21–06; Fig. 14, Tab. 1) differs, with sharp quartz peaks (~31° and 24.22° 2θ) and a weak low-cristobalite peak at ~25.25° 2θ. The other sample (no. 18–04; Fig. 14) is intermediate, showing a strong quartz peak (~30.80° 2θ) and double peaks (~23.99° and 25.03° 2θ) for quartz and low-cristobalite (Fig. 14; Tab. 1). Most samples also display a low-cristobalite peak at ~41.5° 2θ.

Early Cretaceous spicules

The present study is based on a single, exceptionally well-preserved fused hexactinellid skeleton, limiting its analysis to SEM observations.

Fine external sculpture details are visible at low magnification (Fig. 15A, B). Closer examination shows 1–2 µm euhedral quartz microcrystals on the spicule surface (Fig. 15C, D) and within the enlarged axial canal (Fig. 15E). The spicule interior consists of compact silica, made of ~100 nm nanogranules (Fig. 15E, F). No layering is observed, but a central axial canal is present.

Late Jurassic spicules

Both Late Jurassic hexactinellid and lithistid demosponge spicules were studied. The lithistid spicules are exclusively

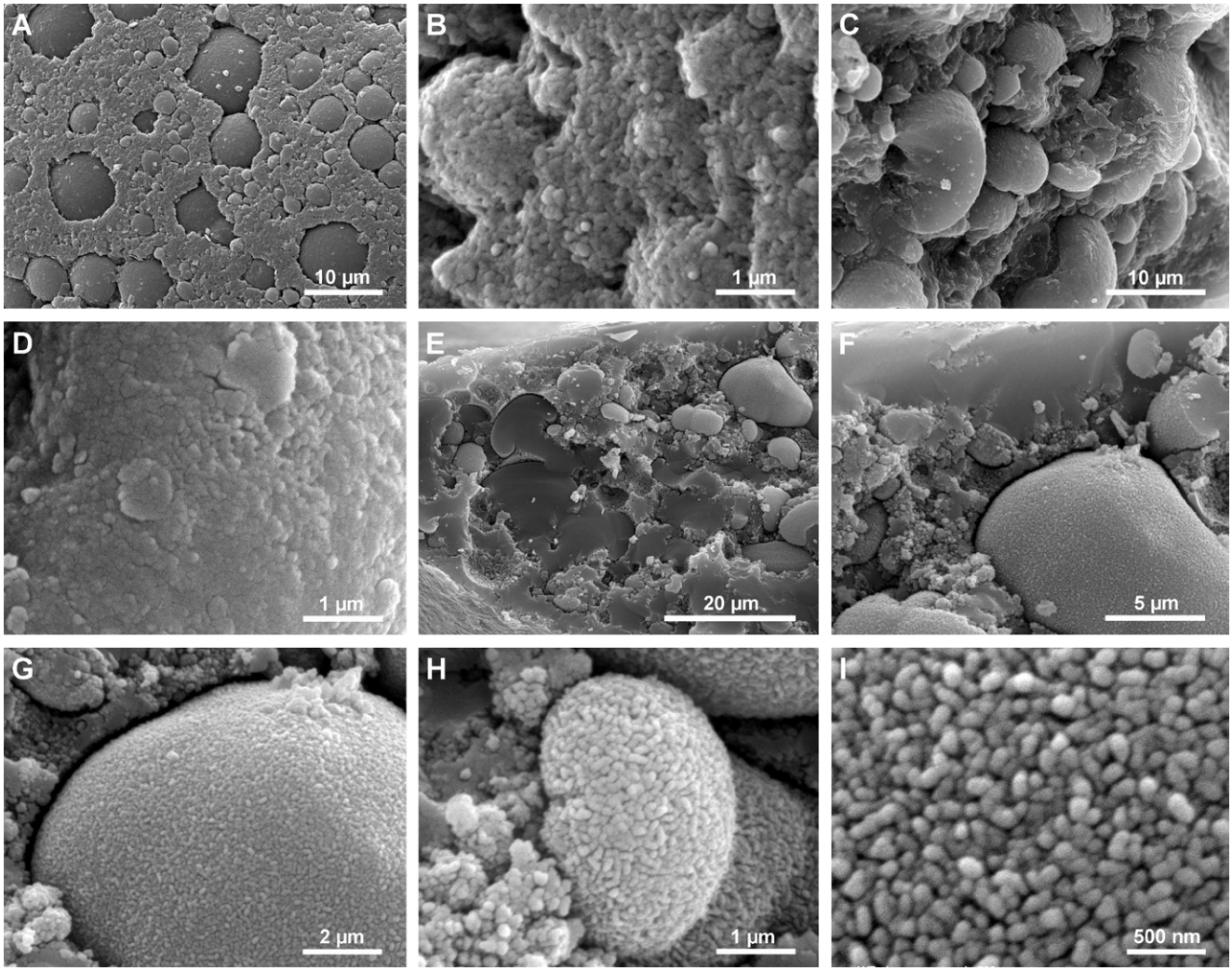

Fig. 5. Eocene opaque spicules of lithistid demosponge (*Pleroma*), SW Australia. **A.** Surface of an opaque spicule, showing an outer layer composed of nano- and microspheres, interspersed with larger microspheres from the spicule's interior. **B.** Close-up of (A), highlighting nanogranules and microspheres (composed of nanogranules) in the outer layer of the spicule, with some clustering of nanogranules visible. **C.** Transverse broken surface, revealing microspheres of various shapes and sizes, embedded in a nanogranular matrix. **D.** Magnified view of microspheres from (C), showing their nanogranular composition. **E, F.** Broken cross-section of the spicules, displaying numerous hemispheres and spheres of silica embedded in a silica nanogranules matrix. **G.** Surface details of a microsphere from (F), showing its nanogranular composition. **H, I.** Detailed views of another microsphere's surface, revealing both nanorods and nanogranules of silica.

rhizoclones, originally lacking an axial canal. Their morphology is generally well-preserved, with intact spines in some areas and rough, porous surfaces elsewhere, showing irregular nanogranule clusters (~100 nm) and larger aggregates (Fig. 16D, E). Rhizoclone cross-sections reveal a dense outer rim (~5 µm thick) of nanogranules and their clusters, with a more porous interior, composed of sharp-edged nanogranule clusters (70–150 nm; Fig. 16F). These spicules are frequently embedded in silica deposits (chert), exhibiting incipient crystalline faces (Fig. 16A–C). Natural spicule surfaces in some cases show aligned silica nanogranules (Fig. 17), resembling those in Late Cretaceous spicules.

Hexactinellid spicules (from a dictyonal fused skeleton) are from well-preserved specimens with intricate surface details. Different preservation stages coexist within fragments, from pristine to strongly etched areas (Fig. 18A). Axial canals are often enlarged but well-defined (Fig. 18E). Surfaces range from rough (Fig. 18B) with incipient microquartz units (~1–1.5 µm; Fig. 18C) to smooth in less corroded zones (Fig. 18D) that at high magnification shows a compact nanogranular structure with nanogranules (~150–200 nm). Such compact zones in cross-section display an outer compact crust (~3 µm thick) with faint layering (Fig. 18E, F), and a porous core with nano- to microclusters (0.7–1 µm) composed of clustered nanogranules (70–100 nm; Fig. 18E, F). In some regions, both exterior and interior reveal incipient microquartz crystals (~0.5–1 µm), formed of nanogranules (90–140 nm; Fig. 18H, I). In another specimen, no internal structure is preserved; these spicules are highly porous, containing irregular hemi/microspheres internally (Fig. 16G, H), and an outer layer of euhedral nanoquartz (500–750 nm), mixed with silica nanogranules (~100–250 nm; Fig. 16I).

The majority of the samples exhibited X-ray diffractograms with primary strong peaks at approximately

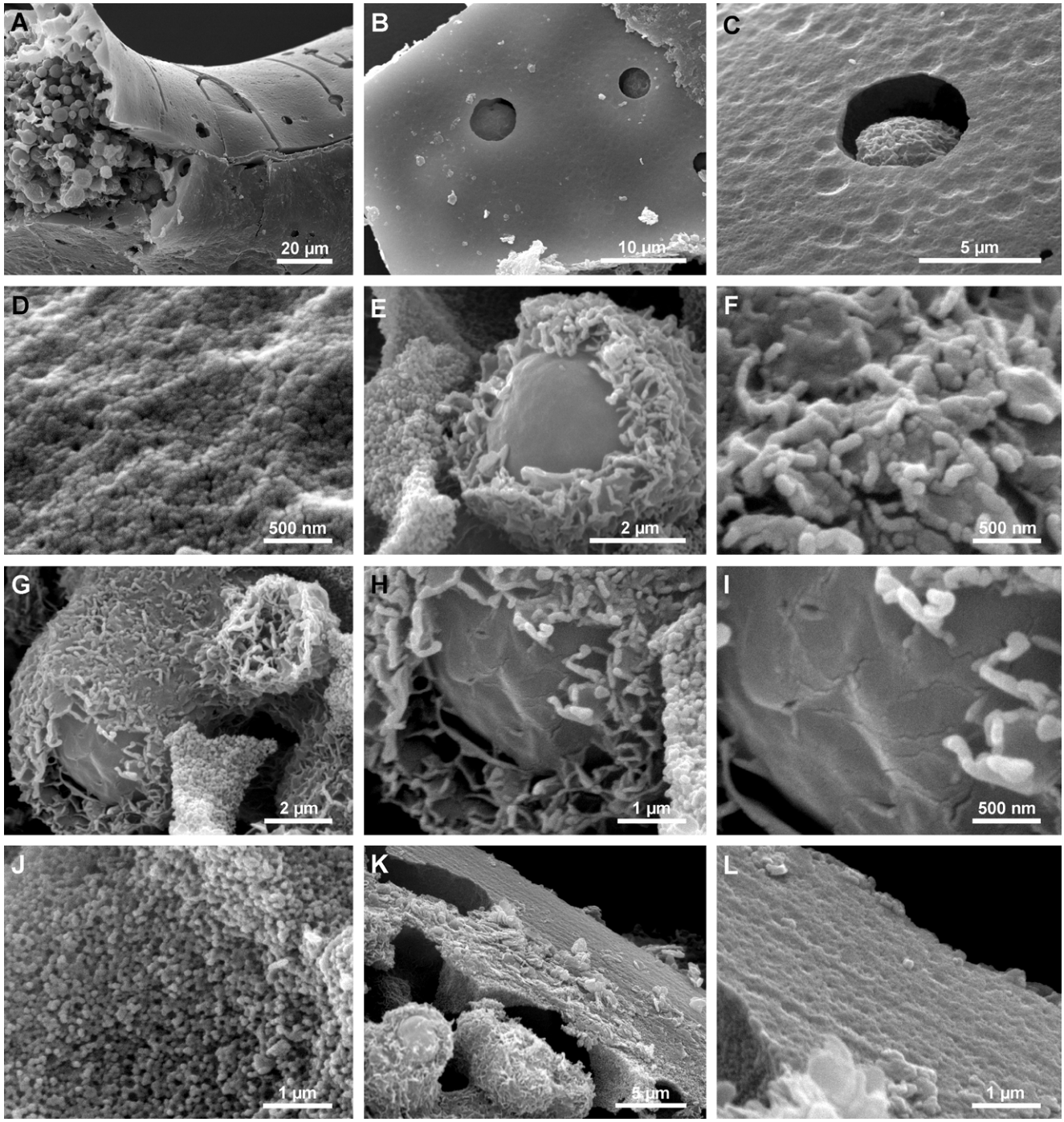

Fig. 6. Eocene white spicules of a lithistid demosponge (*Pleroma*), after etching in NaOH, SW Australia. **A.** Broken cross-section of the spicule, revealing numerous microspheres. **B.** Smooth surface of the same spicule, showing round holes with microspheres visible inside. **C.** Close-up of (B), highlighting the etched surface and microspheres forming the interior. **D.** Enlarged view of the outer layer of the spicule, showing visible nanogranules. **E.** Microsphere within the spicule's interior; its core appears amorphous, while the outer part consists of aligned nanogranules in vermiform chains, resembling but less organized than the blades in lepispheres. Remnants of the silica nanogranules matrix are also visible. **F.** Surface details of the spheres from (E), showing an irregular arrangement of nanogranules in vermiform chains. **G.** Large microsphere (left), similar to (F), along with smaller microspheres (top right), composed entirely of aligned nanogranules. Remnants of the nanogranular matrix are visible at the bottom centre. **H.** Detailed view of the sphere from (F), showing an amorphous centre and a porous outer layer, composed of irregularly aligned nanogranules, possibly forming incipient hemisphere blades. **I.** Central part of the spheres from (G) and (H), highlighting their amorphous nature. **J.** Nanogranular matrix embedding the microspheres. **K.** Marginal section of the spicules, showing microspheres within solid silica and a clearly layered outer structure. **L.** Close-up of the outermost spicule layer, showing layering and nanogranules.

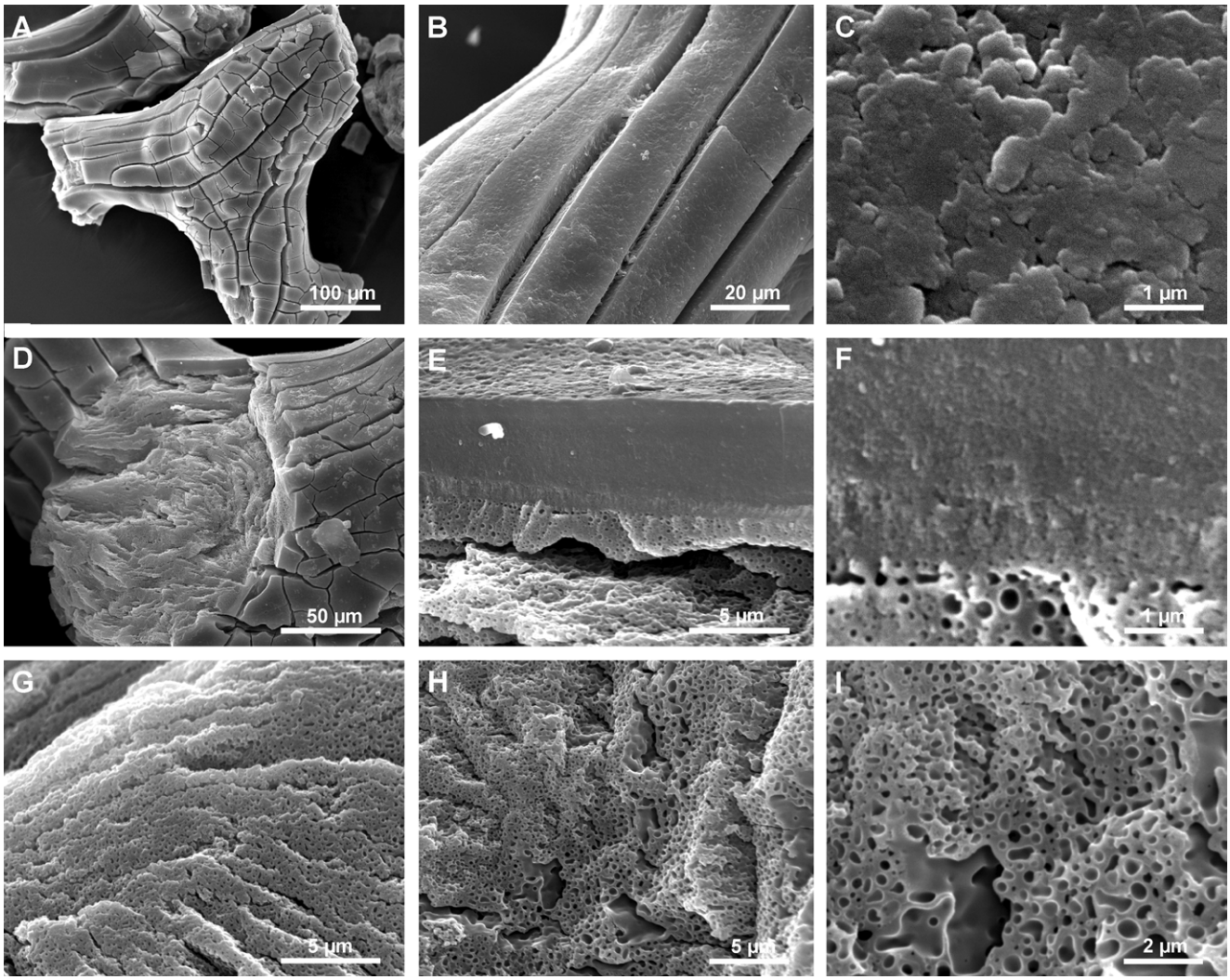

Fig. 7. Eocene lithistid demosponge *Pleroma* spicules, from SW Australia, interpreted as affected by bush fire. **A.** External view of spicules, showing a cracked surface. **B.** Close-up of surface cracks in the spicules. **C.** Silica structure on the spicule surface, highlighting irregular silica units, formed by coalescing nanogranules. **D.** Broken cross-section, revealing distinct silica structures: a denser, cracked outer zone and a layered inner zone. **E.** Magnified view of (D), showing the boundary between the outer and inner zones; the outer zone consists of very dense silica, while the inner zone exhibits nanoporosity. **F.** Detailed view of the boundary, emphasizing the contrast between the dense silica nanogranules of the outer zone and the porous silica of the inner zone. **G.** Further details of the boundary, reinforcing the distinction between the dense outer zone and the porous inner zone. **H, I.** Interior details of the spicules, revealing a 'spongy' structure with nanoporosity; apart from this, the silica appears amorphous.

30.81–31.84° 2Θ with narrow FWHM and d-spacing (Fig. 19; Tab. 1), corresponding to quartz. An additional peak around 58° 2Θ, characteristic of quartz, is also observed, along with a weak peak near 42° 2Θ, indicative of low-cristobalite. Two samples (no. 21-03 and 18-02; Fig. 19; Tab. 1) show divergent patterns, marked by two distinct broad peaks at 23.90–24.22° and 25.14–25.23° 2Θ, plus a low-intensity peak around 42° 2Θ (≈2.50 Å), characteristic of opal-CT (Jones and Segnit, 1971; Elzea *et al.*, 1994). A narrow quartz peak at 30.81–31.84° 2Θ (3.35 Å) is also present.

The diagenetic silica precipitate (sample no. ZA-4), featuring a cauliflower surface with embedded spicules (Fig. 16A–C), shows a sharp quartz peak at 30.84° 2Θ and a smaller, very narrow peak at 24.06° 2Θ (Fig. 19; Tab. 1). A weak peak near 22.4° 2Θ (d=4.6 Å; not shown), interpreted as moganite (Rodgers and Cressey, 2001; Sitarz *et al.*, 2014), appears in this sample and in some quartz spicule samples.

DISCUSSION

Recent spicules

In Recent sponge spicules, the axial canal may appear round due to etching of organic material during preparation. In fossil spicules, axial canals are typically larger and more rounded (Figs 7, 12), reflecting diagenetic removal of silica from the canal walls. This process, linked to their higher organic content and less massive silica, renders these regions more susceptible to alteration. High porosity in the central parts of lithistid spicules treated with HNO_3 supports the idea that this porosity results from the

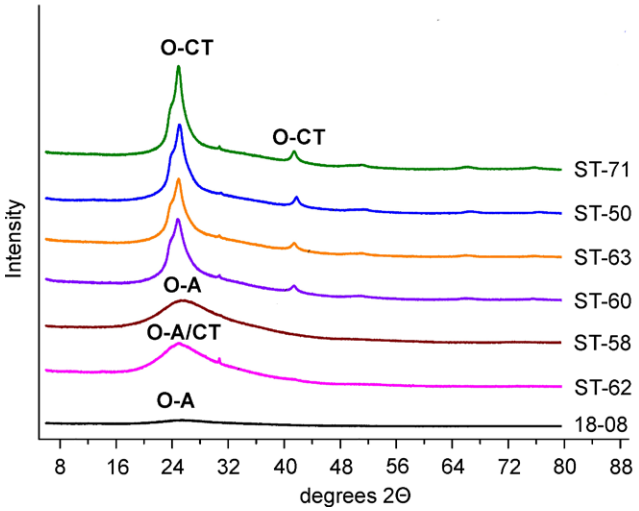

Fig. 8. Typical selected X-ray diffractograms of Eocene spicules from SW Australia (for sample characteristic see Table 1). O-A opal-A, O-CT opal-CT.

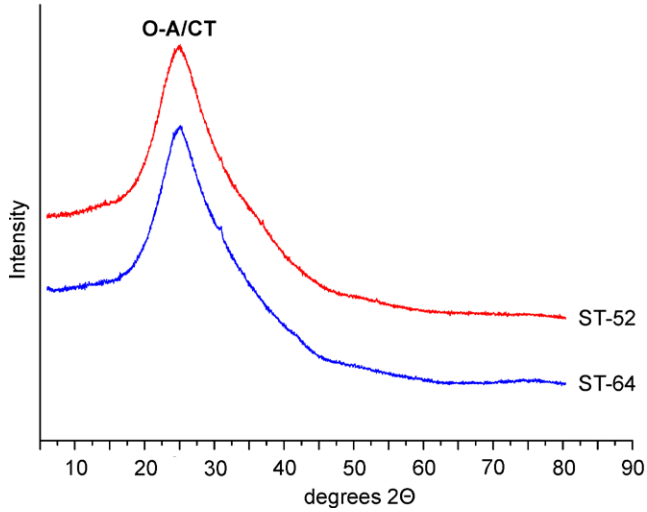

Fig. 9. X-ray diffractograms of the white iridescent Eocene spicules from SW Australia (for sample characteristic see Table 1). O-A opal-A.

oxidation of organic matter. Under SEM, this porous core in lithistid spicules corresponds to the brownish, murky zone, seen in transmitted light microscopy (Pisera, 2003).

XRD studies on Recent sponge spicules are limited by insufficient details (Sandford, 2003) or generalization, focusing only on broad opal-A peaks without specific parameters (Masse *et al.*, 2016; Arasuna *et al.*, 2018), with the exception of Stamm *et al.* (2025). Most studies indicate that spicules in siliceous sponges are composed of opal-A. In contrast, Dudik *et al.* (2021) reported cristobalite, but after calcination at 800 °C for six hours, a treatment that is known to transform opal-A into low-cristobalite (Xue *et al.*, 2015).

In sedimentary opal-A, broad peaks are centred at 3.93–4.13 Å (Elzea *et al.*, 1994; Elzea and Rice, 1996; Herdianita *et al.*, 2000a, b; Lynne and Campbell, 2003, 2004; Rodgers *et al.*, 2004; Lynne *et al.*, 2005, 2007, 2008; Ghisoli *et al.*, 2010; Liesegang and Milke, 2014; Liesegang *et al.*, 2018). All Recent spicules studied show highly consistent parameters, regardless of taxonomy (Tab. 1), indicating no taxonomic control over mineralogy. NMR studies also reveal similar silica condensation levels (Masse *et al.*, 2016). However, Recent spicules show slightly lower FWHM values than those of sedimentary opal-A, with peak positions at lower angles and higher d-spacing. This may reflect their nature as biocomposites, rather than pure silica (Ehrlich and Worch, 2007; Ehrlich *et al.*, 2008; Müller *et al.*, 2008; Wang *et al.*, 2010). The FWHM values of the studied spicules fit very well with those reported by Stamm *et al.* (2025), but the d-spacing values are slightly higher, consistently above 4 Å.

Eocene spicules

Opal-A in glassy/translucent spicules (Tab. 1; Figs 8, 11) show FWHM values slightly lower than in Recent spicules, but d-spacing values higher, suggesting early mineralogical reordering, despite the lack of obvious morphological modifications. Surface corrosion likely results from diagenetic etching or early marine dissolution (Bertolino *et al.*, 2017).

Sample ST-62, also glassy, displays intermediate parameters between opal-A and opal-CT (Tab. 1), interpreted as a mix, dominated by opal-A (Graetsch *et al.*, 1987; Graetsch, 1994; Lynne and Campbell, 2004; Rodgers *et al.*, 2004; Lynne *et al.*, 2005, 2008; Liesegang *et al.*, 2018). Lynne *et al.* (2007) linked such diffractograms to aligned nanogranules (opal-CT), but we suggest that these reflect coexisting micropatches of opal-A and opal-CT, supported by glass-like and granular domains within single samples (Figs 3F, G; 10I).

SEM and XRD data indicate that the earliest macroscopic sign of silica reordering of opal-A spicules is their transition from translucent to a white or milky appearance. Translucent spicules are compositionally homogeneous (Figs 3A, B; 10A–C); white ones are heterogeneous, with microspheres of various sizes in a nanogranular matrix (Fig. 4A–C). The microspheres cause light refraction at their surfaces, resulting in a milky appearance.

Round surface holes reveal underlying microspheres (Figs 3D, F, G–I; 6B, C), likely formed by internal microsphere growth at the expense of the outer silica, rather than corrosion.

Etching white spicules reveals microspheres with homogeneous cores and outer crusts of aligned nanogranules in vermiform chains (Fig. 6E–I), resembling incipient lepispheres. These are embedded in silica nanogranules, separated from them by narrow voids (Figs 3F–I; 4B, C), suggesting maturation-related reorganization via solid state (no involvement of dissolution and precipitation in a void) transformation.

The transition from opal-A to opal-CT involves water loss and volume reduction (Jones and Renaut, 2007; Jones, 2021), leading to narrow gaps between microspheres and the matrix, and potentially forming nanopores (Fig. 3E, F, I). Similar nanogranule alignment during

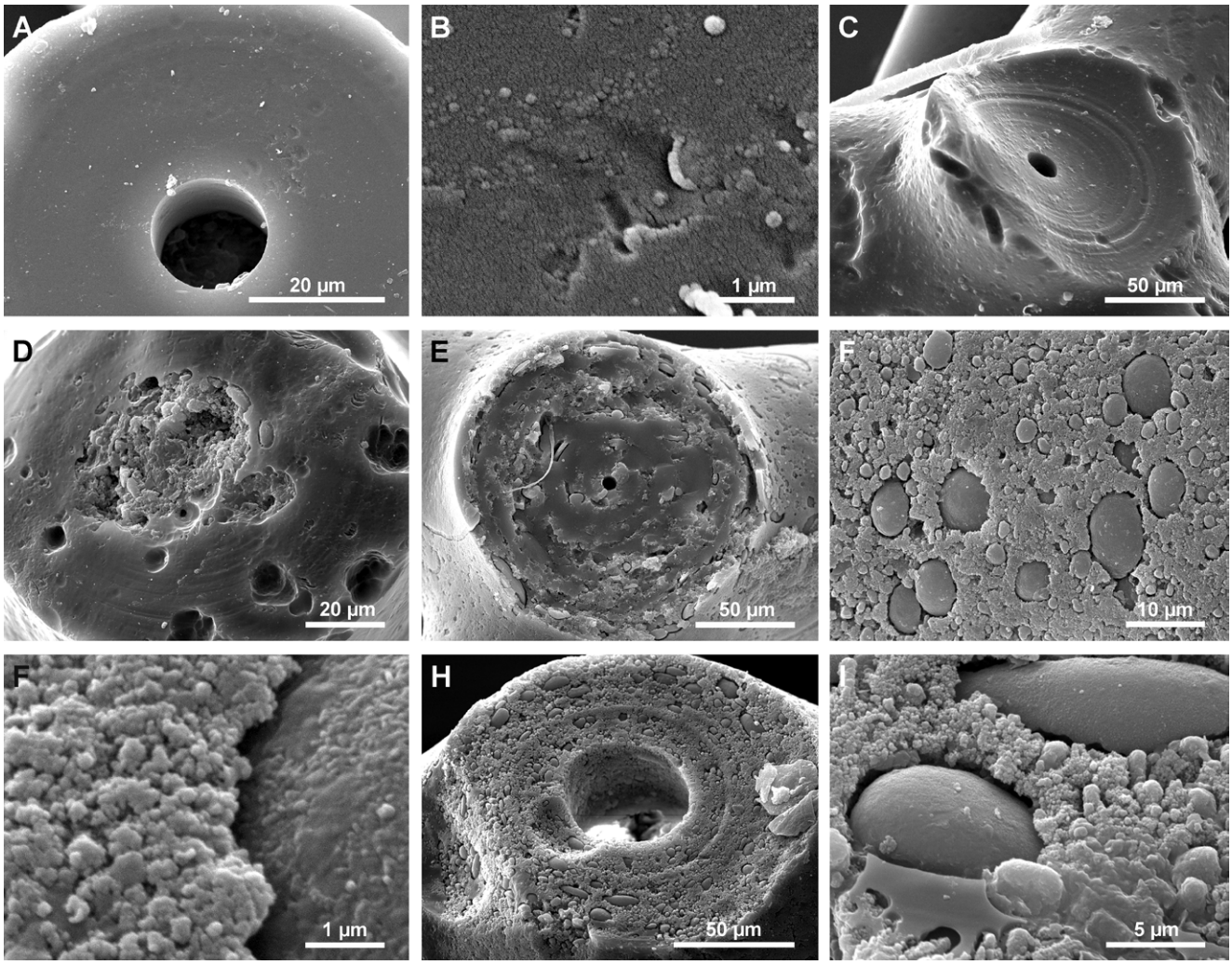

Fig. 10. Eocene demosponge spicules from Ukraine. **A–C.** Cross-section of a translucent (glassy) soft demosponge spicule composed of amorphous silica (B). A round axial canal is visible (A, C), along with traces of original layering. **D, E.** Cross-section of white spicules with a modified axial canal (E). Smooth (glassy) silica coexists with granular silica (microspheres). The centre of the spicules is strongly modified and composed of granular silica, while the outer part remains structureless and retains traces (D) of the original layering. **F.** Surface of a white (milky) spicule, showing larger microspheres from the interior visible through surface holes, which are composed of smaller micro- and nanogranules. **G.** Coalescing aggregation of nanogranules, forming the spicule's surface layer, along with large interior microspheres composed of nanorods. **H.** Natural section of a white (milky) spicule, where traces of the original layering remain. The axial canal is greatly enlarged, while the spicule consists of larger microspheres of varying diameters, similar to (F–G) and coalescing aggregates of nanogranules**. I.** Natural cross-section, showing a large microsphere, composed of nanogranules, embedded in a matrix of coalescing aggregates; remnants of smooth (glassy) silica are visible in the lower left.

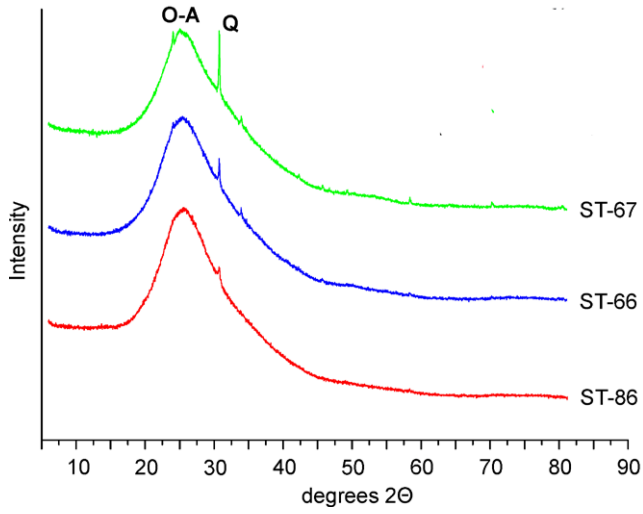

Fig. 11. Typical selected X-ray diffractograms of Eocene spicules from Ukraine (for sample characteristic see Table 1). O-A opal-A, Q quartz.

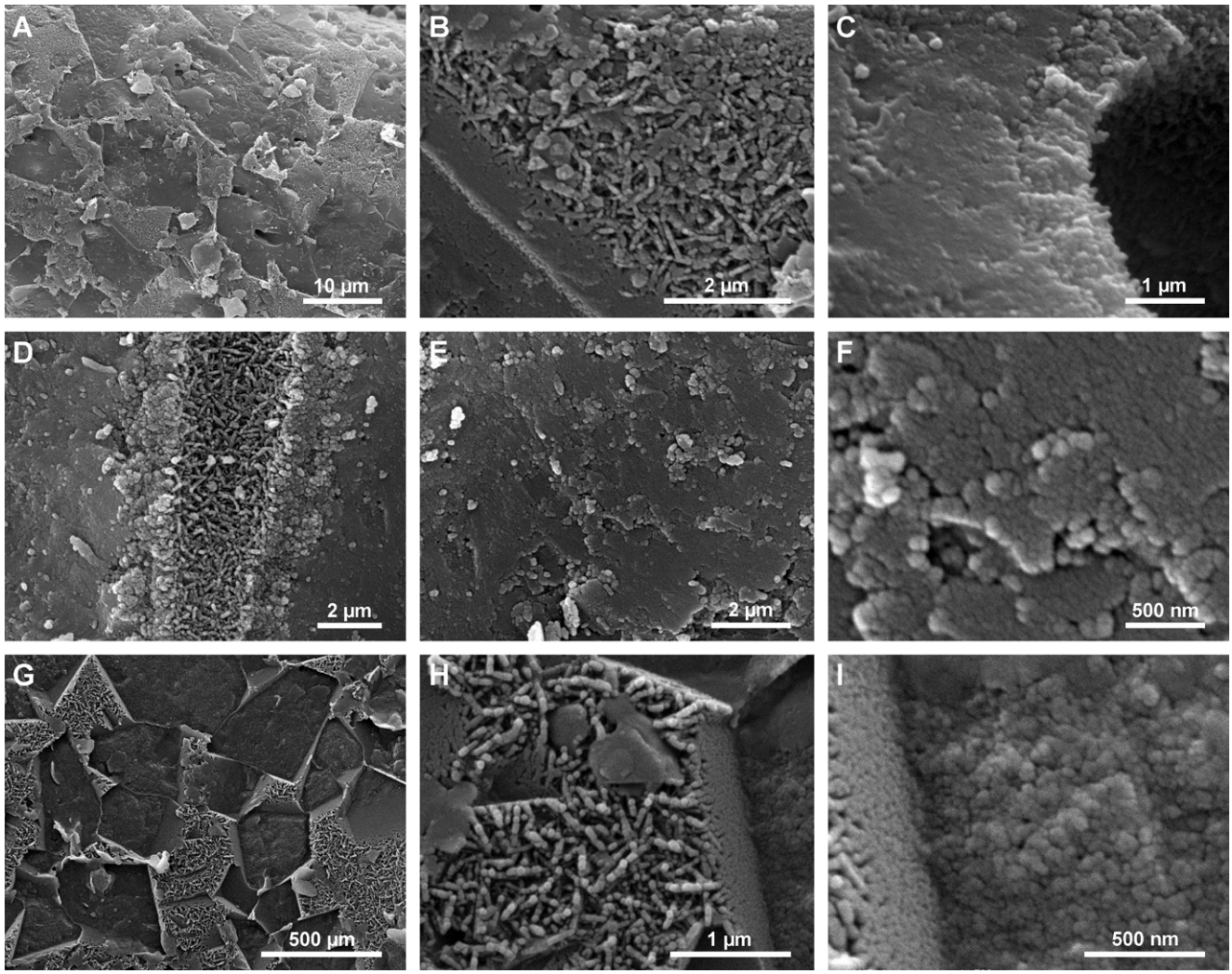

Fig. 12. Late Cretaceous hexactinellid spicules and lithistid demosponge spicules from Germany. **A, B.** Surface of the hexactinellid spicule, showing impressions of calcite crystals. Between these impressions, the spicule surface features criss-crossing silica blades similar to those in lepispheres (B), composed of linearly arranged nanogranules. **C.** Transverse section of the spicule, highlighting the difference between the marginal zone of the axial canal (right), which consists of silica blades, and the central solid part of the spicule (left), composed of nanogranules. **D.** Longitudinal section of the axial canal, revealing irregularly arranged silica blades, composed of nanogranules, corresponding to the right zone in (C). **E, F.** Silica structure of the central part of the spicule, seen as large blocks (E) composed of silica nanogranules (F). **G–I.** Surface of the lithistid demosponge spicule, showing imprints of calcite crystals (G); between these, the natural surface (raised elements) features bladed silica composed of linearly arranged nanogranules similar to those in lepispheres (H). Silica nanogranules are visible on the smooth surface between bladed silica, corresponding to (E).

opal-A reorganization into opal-CT has been observed in sinters (Lynne *et al*., 2005).

Silica microspheres and microhemispheres in nanogranular matrices – seen in modified Eocene spicules from Australia – resemble structures from New Zealand sinters (Jones, 2021), previously interpreted as opal-A in opaline cement. However, XRD confirms these Australian spicules are opal-CT, indicating a diagenetic origin. Unlike sinter cements, the opal-CT formed internally within spicules via nanoscale reorganization, without signs of dissolution or reprecipitation – a process akin to silica "neomorphism," similar to calcium carbonate neomorphism (Du and Amstad, 2020). This transformation may parallel the "sphere pathway" of opal-A to quartz (Lynne and Campbell, 2004), though, unlike hollow sinter spheres, the spicule microspheres are solid.

Milky (altered) and translucent (unaltered) silica can coexist within one specimen or even a single spicule – also observed in the Eocene spicules from Italy (Frisone *et al*., 2014) – implying dominant intrinsic, rather than environmental control. Microspheres form internally within a matrix of nanogranules, not externally, indicating that diagenesis initiates from the porous centre rather than outside, progressing in a nearly closed system of a spicule via solid-state transformation. In the case of dissolution and reprecipitation, dissolution must start at the surface (with diagenetic fluids originating from the surrounding sediments) and progress toward the centre.

Diffractograms of such spicules show broad peaks with shoulders toward lower angles, FWHM 1.584°2Θ, and d-spacing 4.157 Å (Tab. 1).

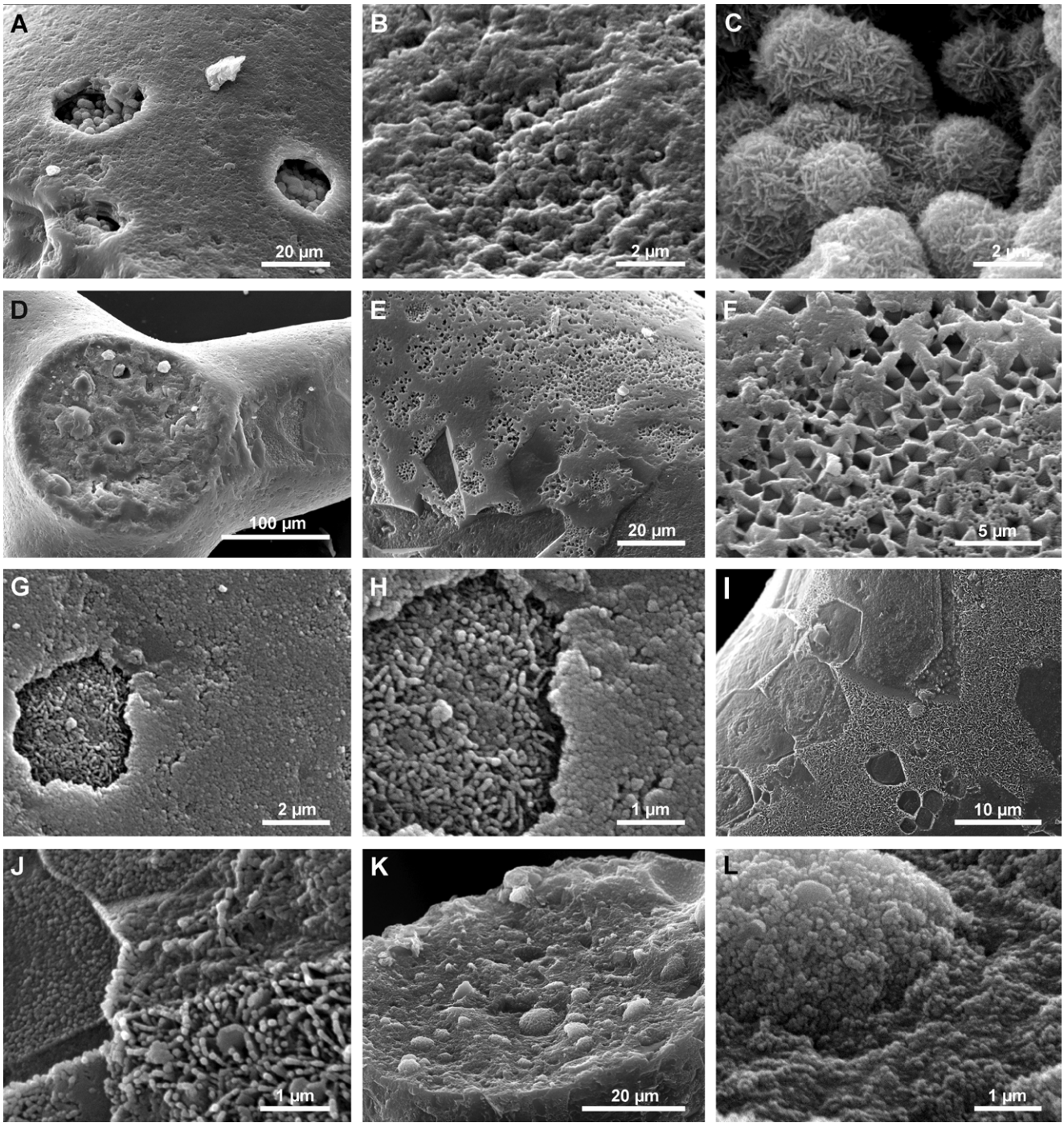

Fig. 13. Late Cretaceous spicules of soft demosponge and lithistid demosponge from Germany. **A.** Surface of the spicule displaying round holes through which lepispheres from the interior are visible. **B.** Detailed view of the surface showing nanogranules and coalesced nanogranules. **C.** Enlarged view of lepispheres inside the spicule (from (A)) with well-developed blades. **D.** Cross-section of the spicule, revealing an enlarged rounded axial canal and the absence of other original structures. **E**. Surface of the spicule with imprints of various diagenetic (probably dolomite) crystals (both small and large) from the host sediment. **F.** Close-up of (E), highlighting the silica nanogranules forming the spicule. **G.** Surface of a lithistid spicule, showing round holes with incipient lepispheres from the spicule interior. **H.** Detailed view of (G), showing nanogranules and coalesced nanogranules in the external layer of the spicule, along with aligned nanogranules in the incipient lepisphere. **I.** Another lithistid spicule with imprints of diagenetic calcite crystals from the host rock; note the bladed silica on the elevated (original) surface of the spicule. **J.** Close-up of (I), showing incipient silica blades, composed of aligned nanogranules (elevated elements) alongside nanogranules characterizing the spicule interior (depressions in the spicule surface). **K.** Broken transverse section of the spicule, revealing numerous microspheres and the absence of original structures. **L.** Close-up of (K), showing that both the matrix (right) and the microspheres (left) are composed of similar nanogranules.

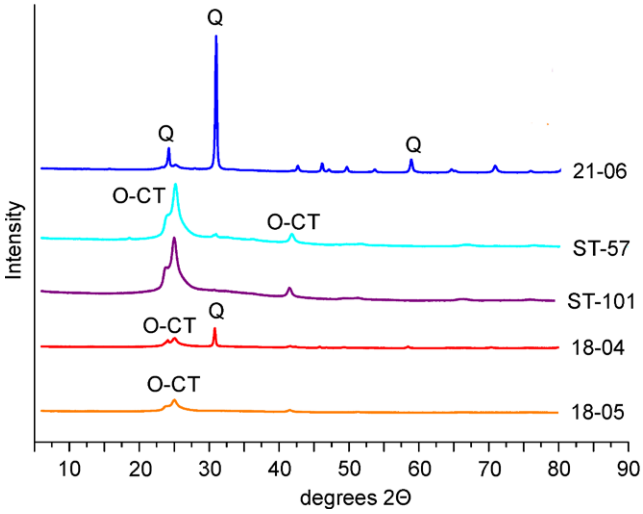

Fig. 14. Typical selected X-ray diffractograms of Upper Cretaceous spicules from Germany (for sample characteristic see Table 1). O-CT opal-CT, Q quartz.

Advanced diagenesis yields opaque spicules (e.g. ST-63, ST-71, ST-50) with broad XRD peaks, weak shoulders toward lower angles, and FWHM/d-spacing typical of opal-CT (Fig. 8; Table 1). Lower FWHM values than milky spicules suggest a later diagenetic stage of opaque spicules. SEM shows rough surfaces with intersecting microspheres (Figs 3D, 5A), and interiors are dominated by irregular nanogranule-based spheres (Fig. 5C, E, I), indicating a distinct diagenetic pathway, possibly influenced by structural factors.

A unique case involves iridescent spicules, derived from a single specimen that is blackened at the surface, as are the rocks that were exposed to fire. The spicules display fissured surfaces and spongy interiors, resembling textures produced by acetylene-flame heating (Wang *et al*., 2010). We link these features to bushfire, traces of which we observed in the field (confirmed by a park ranger) in the area, where the specimen was collected. During such bushfires, temperatures may briefly rise to 800–1,500 °C (DeBano, 1998). Most likely, the interiors of the spicules – richer in organics and composed of larger granules – were more strongly altered by high temperatures, whereas the denser, less porous exterior remained relatively intact, but became fissured. These spicules exhibit broad XRD signals with high FWHM (opal-A) and d-spacing values indicative of opal-CT (Fig. 9; Tab. 1), resembling opal-A samples heated to 1,050 °C (Liesegang *et al*., 2018).

Most Ukrainian translucent spicules yield XRD patterns consistent with opal-A (Fig. 11), with slightly higher FWHM than their Australian counterparts, suggesting lower diagenetic alteration. SEM studies confirm this, showing homogeneous, amorphous silica (Fig. 10A–C). Some spicules (Fig. 10D–I), however, show advanced transformation – microspheres and nanogranules form a matrix, similar to the opaque Australian examples. Limited sample volume restricts further XRD analysis, but even highly altered spicules often retain patches of homogeneous silica (likely opal-A), particularly in the less altered outer regions, supporting the internal initiation of diagenesis.

Late Cretaceous spicules

Demosponge spicules are primarily composed of opal-CT with minor quartz, as shown by XRD data (Tab. 1). Some exhibit d-spacing values slightly lower than those

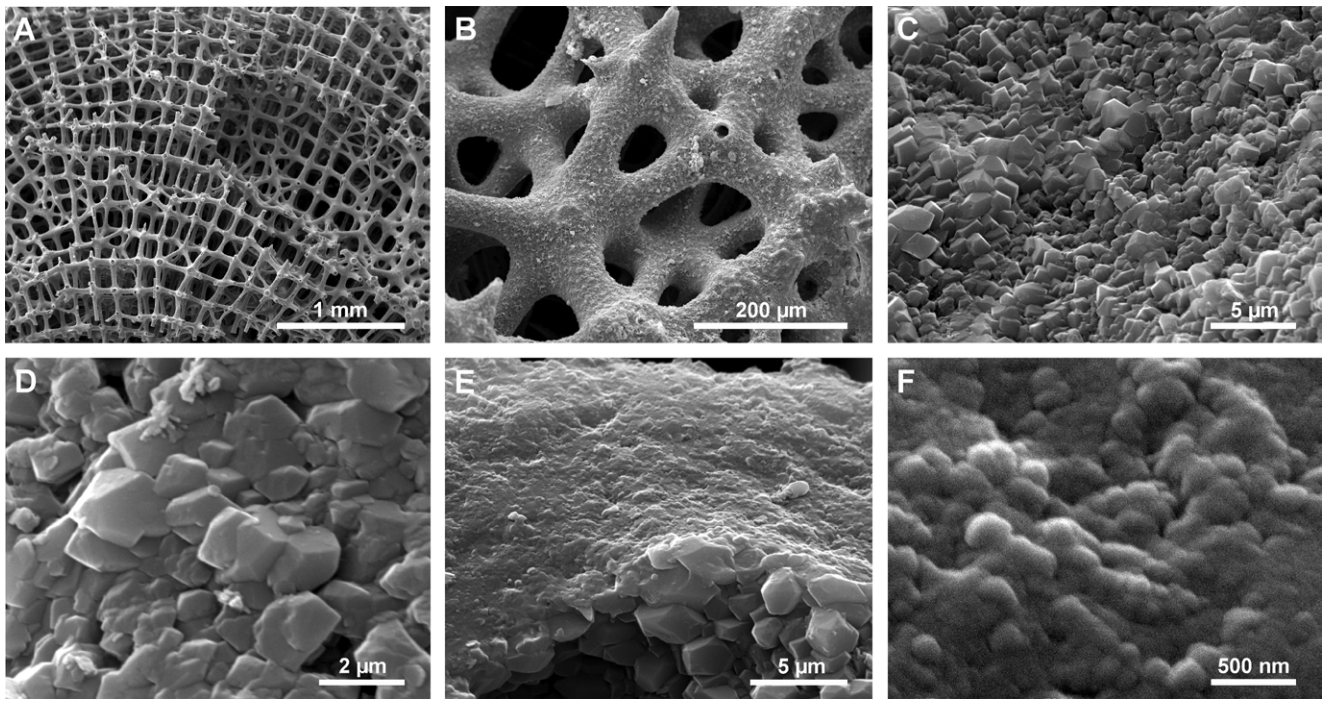

Fig. 15. Lower Cretaceous hexactinellid spicules from Spain. **A, B.** Well-preserved hexactinellid skeleton, with even the finest details of the spicule sculpture intact. **C, D.** Well-developed microcrystalline quartz on the spicule surface. **E, F.** Broken section, showing microcrystalline quartz on the surface of the axial canal (E) and massive silica, composed of nanogranules forming the spicule interior (F).

of the Eocene opal-CT spicules, but significantly reduced FWHM values indicate more advanced diagenesis. A more pronounced shoulder toward lower angles at ~4.10 Å, compared to the Eocene Australian samples, further reflects silica maturation.

Hexactinellid spicules (samples 21-06, 18-04; Fig. 14; Tab. 1) show the most advanced diagenesis, with quartz as the dominant phase and minor opal-CT. Internally, they consist of massive, poorly defined units, composed of nanogranules (Fig. 12C, E, I), consistent with quartz. In contrast, aligned nanogranules, forming criss-cross bladed structures on surfaces and within axial canals (Fig. 12B, G, H), correspond to opal-CT, fitting the "smooth pathway" model of diagenesis (Lynne and Campbell, 2004).

Regular angular surface depressions are interpreted as imprints of diagenetic calcite and/or dolomite crystals from the host rock. Microspheres, composed of aligned nanogranules, represent early lepisphere formation (Fig. 13F–I), while some spicules show fully developed lepispheres (Fig. 13C) inside, and others contain microspheres, embedded in a nanogranular matrix (Fig. 13K, L). The coexistence of various silica transformation stages within spicules of the same age and from the same lithology is another proof of the microscale of diagenetic processes.

Because the Late Cretaceous spicules are from museum collections, their precise geological context is unknown. Thus, it remains unclear whether diagenetic differences between demosponge and hexactinellid spicules reflect taxonomy or varying preservation conditions, though Jurassic spicules suggest that the differences are associated with the lithology of the host rock. Similar silica structures, microspheres and lepispheres, as discussed above, were described

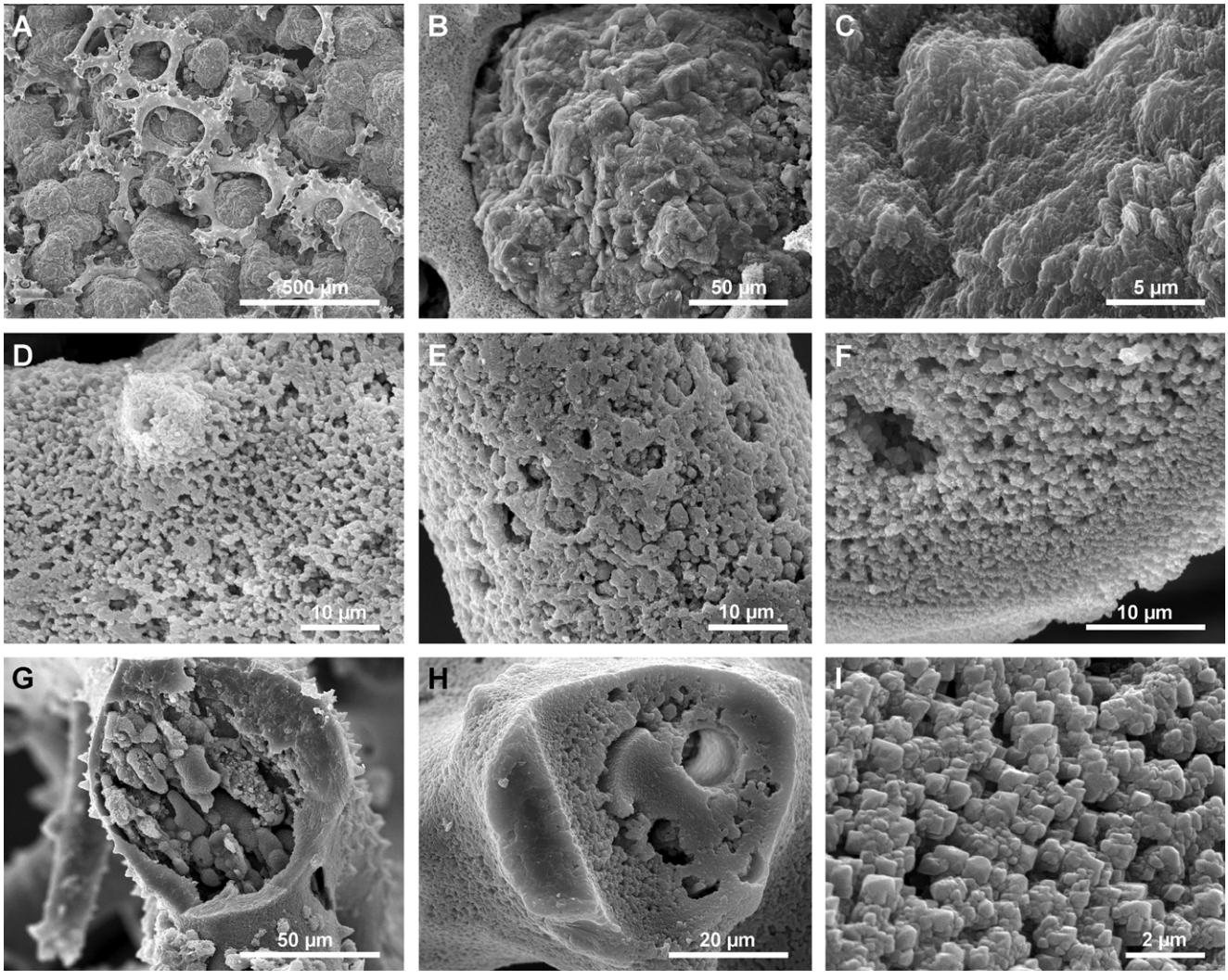

Fig. 16. Late Jurassic spicules (desmas) of demosponges and hexactinellids from Poland. **A.** Rhizoclone desmas, embedded in diagenetic silica deposit with cauliflower surface. **B, C.** Close-up of diagenetic silica between the desmas shown in (A), revealing units, composed of poorly crystalline (incipient quartz) aggregates nanogranules and nanorods. **D, E.** Rough, porous desma surfaces, revealing poorly crystalline (incipient quartz) aggregates (D) and larger microspheres inside the spicule, visible beneath the surface (E). **F.** Broken cross-section of a spicule, showing a denser exterior zone and a porous interior zone composed of microgranular quartz. **G.** Broken cross-section of a desma with a completely obliterated original structure, displaying irregular microspheres; note the dense outer silica layer. **H.** Broken cross-section of a spicule with its original structure completely obliterated, showing various silica microaggregates, including microspheres (right) and microquartz (left). **I.** Close-up of (H) (left), showing incipient microquartz crystals and nanogranules interspersed between them.

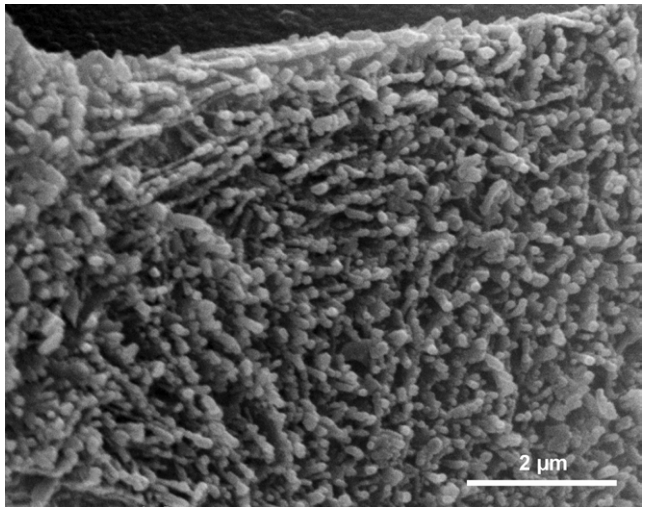

Fig. 17. Natural surface of a Late Jurassic hexactinellid sponge with aligned silica nanogranules.

in the Cretaceous spicules from Poland (Jurkowska and Świerczewska-Gładysz, 2020, fig. 7A, B; Jurkowska *et al*., 2026, fig. 2E, F, H). However, they were misidentified as "botryoidal aggregates" on external surfaces, despite images showing internal locations. This may appear to be an insignificant mistake, but in fact it can influence the interpretation of the diagenetic sequence, thereby causing doubts about the proposed diagenetic scenario. These issues are not further discussed here for consistency, and will be approached elsewhere, because they are important for understanding the diagenetic sequence of spicule-bearing rocks.

The Late Cretaceous spicules studied are clearly more advanced diagenetically than those described by Stamm *et al.* (2025), as indicated by the fact that many of their spicules are translucent and composed of opal-A. In this respect, the diagenetic advancement of the Cretaceous spicules studied by Stamm *et al.* (2025) can be compared with the diagenetic stage of the Eocene spicules of the present study. This is most likely due to the fact that their spicules were continuously covered by seawater, thus remaining isolated from atmospheric influences and elevated temperatures.

Interestingly, the FWHM values of many Cretaceous spicules examined by Stamm *et al.* (2025) are higher than those of their Recent spicules, which is difficult to interpret, since FWHM values systematically decrease with increasing crystallinity. In this context, it would suggest that their Recent spicules consist of a more ordered form of silica than the fossil ones – a rather paradoxical conclusion.

Early Cretaceous spicules

Despite the preservation of fine surface details (Fig. 15A–D), spicules are preserved as massive silica with a nanogranular structure (Fig. 15E, F), likely quartz. This indicates more advanced diagenesis, compared to Late Cretaceous and even some Late Jurassic spicules, due to their exposure to burial conditions with high pressure and temperature, associated with tectonic processes in the Southern Pyrenees.

Late Jurassic spicules

The rough surface of the Jurassic spicules results mainly from a porous outer layer of microgranular or microcrystalline silica (Fig. 16D, E), though some spicules are also deeply etched. XRD analysis confirms that these spicules are predominantly quartz, with some also containing opal-CT (Tab. 1; Fig. 19). Minor amounts of moganite and low-cristobalite were detected via XRD, with low-cristobalite also seen in SEM images (Fig. 18C). Moganite has similarly been reported in 1,900-year-old sinters from Utah (Lynne *et al*., 2005) and in Jurassic sponge limestones in Poland (Kochman and Matyszkiewicz, 2023).

Mineralogical differences do not correlate with spicule type or taxonomy. For example, both hexactinellid and lithistid (rhizoclone) demosponge spicules from the Zalas marls contain a mixture of opal-CT and quartz, whereas other rhizoclones from the same site are composed exclusively of quartz. Even within a single hexactinellid specimen, spicules may vary significantly – some retain detailed sculpture, while others are heavily etched – highlighting the micro-scale variability of diagenesis.

The opal-CT in these spicules shows distinct low-tridymite and low-cristobalite peaks (Fig. 19) and is linked to less advanced diagenesis in marl deposits. Opal-CT is absent from limestone-hosted spicules, regardless of taxonomy. SEM imaging suggests that the opal-CT occurs on surfaces of hexactinellid spicules from Zalas, where aligned nanogranular textures are present (Fig. 17). A dense external rim of silica nanogranules, preserving original layering, is also seen in these spicules (Fig. 18E–G), but not in the quartz-dominated specimens from other outcrops.

Quartz is easily recognized in SEM by euhedral nano- and microcrystals (Fig. 16I). A full transition is observed – from irregular nanograin clusters (Fig. 18E, F), to early quartz with faint crystal faces (Fig. 18H, I), to well-formed quartz crystals (Fig. 16I). Nanogranules at the base of these crystals indicate that they formed via diagenetic transformation (fusion) of less-ordered silica. Low-cristobalite in the Jurassic samples is clearly late diagenetic, seen as euhedral crystals on etched spicule surfaces.

Diagenetic silica (chert), embedding many Jurassic spicules likely derives from sponge-origin silica, formed by dissolution of nearby spicules and subsequent *in situ* reprecipitation. Our petrographic studies support this, and the silica matrix shares the same mineralogy as adjacent spicules (Fig. 19; Tab. 1). Its structure – incipient quartz growing from silica nanogranules – suggests initial deposition as opal-CT, followed by transformation to quartz via the same pathway as observed in spicules.

The extensive diagenetic alteration of the Jurassic spicules reflects not just their age, but also deeper burial than that of their younger counterparts. Unlike most younger deposits (except Lower Cretaceous), the Jurassic rocks were later overlain by Cretaceous and Paleogene/Neogene sediments, subjecting them to greater pressure and temperature.

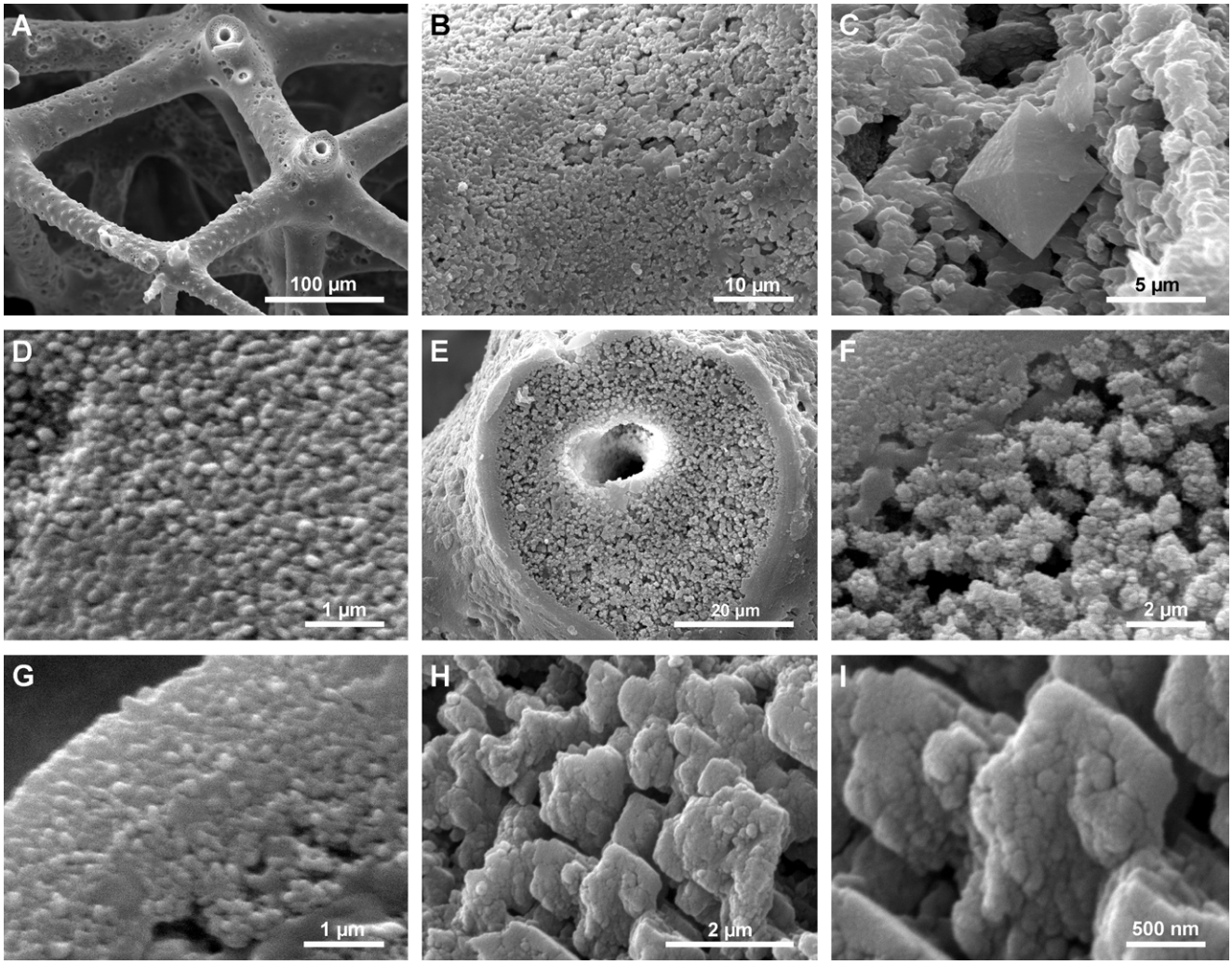

Fig. 18. Late Jurassic hexactinellid spicules from Poland. **A.** Well-preserved skeleton of a hexactinellid sponge, showing an enlarged axial canal, original tuberculation, and smooth silica in some areas, while appearing rough (etched) in others. **B.** Details of the skeleton surface, highlighting irregular coalescing nano- and microgranules (incipient microquartz) and rounded openings in the outer spicule layer, with larger microspheres visible inside the spicule. **C.** Close-up of (B), showing a rough surface with euhedral cristobalite; note how the irregular, complex nano- and microgranules begin to resemble microquartz crystals. **D.** Details of a well-preserved surface, revealing a nanogranular structure. **E.** Cross-section of spicule; enlarged axial canal in centre, note dense outer zone, composed of nanogranules and more porous zone in centre). **F.** Details of central zone from (E) composed of irregular clusters of nano- and microspheres. **G.** Details of outer dense zone from (E), composed of nanogranules, note some evidence of layering. **H, I.** Irregular subcrystalline and poorly crystalline structures (incipient microquartz crystals) (H), composed of nanogranules (I).

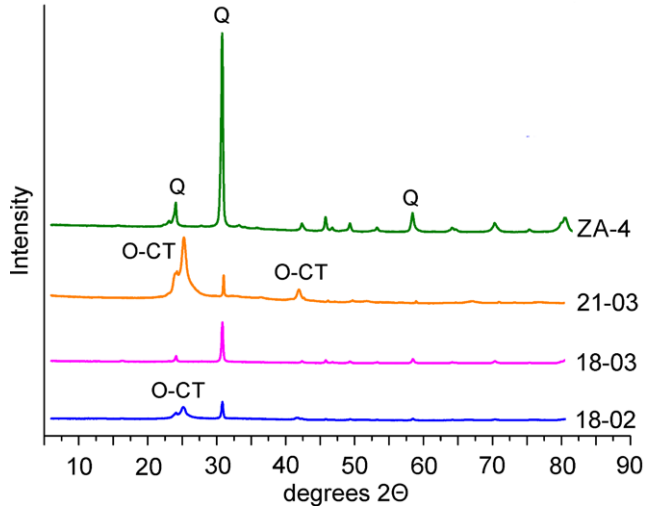

Fig. 19. Typical selected X-ray diffractograms of Upper Jurassic spicules from Poland (for sample characteristic see Table 1). O-CT opal-CT, Q quartz.

General aspects of diagenesis of siliceous spicules

The XRD analysis shows that only the translucent (glassy) Eocene spicules from Ukraine and SW Australia are preserved as opal-A. These spicules come from deposits that were never deeply buried and, therefore, were not subjected to high pressure and temperature. However, their lower FWHM values and higher d-spacing compared to modern spicules suggest that mineralogical changes begin before visible alteration (Lynne and Campbell, 2004).

Eocene spicules within a single sample, or even within a single specimen, in many cases exhibit varying diagenetic stages, ranging from translucent (opal-A) to white, with microspheres indicative of opal-CT formation. Some individual spicules contain both zones: translucent (likely opal-A) and opaque or white (likely opal-CT; cf. Frisone *et al*., 2014; Stamm *et al*., 2025). This suggests that diagenetic transformation is driven more by the mineralogical instability of opal-A at the microscale than by the external sedimentary conditions in such cases, where no high pressure or temperature operated. Similar coexisting silica polymorphs have been observed in sinters (Campbell *et al*., 2001; Lynne and Campbell, 2004; Lynne *et al*., 2005, 2007, 2008).

Most spicules, regardless of age, location, or taxonomy, retain some original structural features. Axial canals, characteristic of hexactinellids and soft demosponges, are usually preserved in the studied spicules, though enlarged. This enlargement is likely due to the originally more porous silica with high organic content near the canal, which is more susceptible to removal during early diagenesis. Spicules (desmas of lithistids), not preserved as opal-A, show preferential alteration of the inner, porous, originally organic-rich zone, while the denser outer part remains less affected. An indicator of early diagenesis is the formation of microspheres, embedded within a nanogranular matrix of similar composition. This relationship suggests that the microspheres replace the matrix, rather than forming in pre-existing voids or being deposited through a dissolution-reprecipitation process. Such a process would be expected to produce a more crystalline phase, i.e., typical lepispheres composed of criss-crossed blades of tridymite, which, however, is not observed in the present study.

Hexactinellid spicules generally appear less well preserved internally than demosponge ones from the same rocks, though this may be an effect of limited sampling. Nevertheless, the lower resistance of modern hexactinellid spicules to dissolution, seen in both nature (Bertolino *et al*., 2017) and lab settings (Maldonado *et al*., 2005, 2022), supports this observation.

The XRD analysis clearly shows gradual silica maturation over time. Fossil opal-A peaks are narrower (lower FWHM) than those of modern spicules (Tab. 1; Figs 2, 8, 11). In the Eocene samples, opal-CT shows a weak shoulder toward lower angles (Fig. 8), which becomes more pronounced in the Cretaceous samples (Fig. 14), eventually forming distinct low-tridymite and low-cristobalite peaks in the Jurassic samples (Fig. 19). The Jurassic opal-CT peaks are also narrower than those of opal-CT in the younger spicules studied.

There are two principal pathways for silica transformation. The first involves dissolution, followed by reprecipitation of more ordered polymorphs, in many cases accompanied by the formation of intermediate spicule moulds (cf. Matysik *et al*., 2018, 2021; Jurkowska and Świerczewska-Gładysz, 2020; Stamm *et al*., 2025; Jurkowska *et al*., 2026; as well as our unpublished data on opoka). This process commonly requires at least partial cementation of the surrounding sediments. The dissolution–reprecipitation model is widely accepted and frequently invoked in geological studies, as mentioned in the Introduction, although it is typically supported by indirect evidence and based largely on observations of silica diagenesis in sediments, rather than direct structural data.

This type of transformation involves sediment pore fluids and proceeds through dissolution of an unstable silica phase, followed by precipitation of a more stable one. As a result, the original internal structure is usually obliterated, although some surface details may occasionally be preserved (Pisera, unpublished). The process operates in a relatively open system and may lead to chemical, including isotopic, fractionation. Consequently, spicules that have undergone such diagenesis should not be used for isotopic studies, aimed at the reconstruction of past environments, as their original isotopic signature is no longer preserved (cf. Slagter *et al*., 2025).

The second pathway is a solid-state transformation, also referred to as silica maturation or gradual ordering of silica (Calvert, 1974, 1977; Murata and Nakata, 1974; Mizutani, 1977; Cady *et al*., 1996). In the case of amorphous silica, this process involves the transformation of one solid phase (opal-A) into another (opal-CT and ultimately quartz), without an intermediate dissolution stage (fluid phase). The transformation proceeds through reorganization of the internal structure, with atomic migration over very short distances within a closed system. As a consequence, the chemical and isotopic compositions remain essentially unchanged. Importantly, this process typically preserves the original internal structure and does not involve mould formation.

This solid-state process of silica maturation most likely proceeds via progressive dehydration of opal-A of sponge spicules, which contains on average 12% water (Sandford, 2003), followed by fusion or, more precisely, sintering of silica [for definitions and theoretical background, see Kang (2004)]. Sintering refers to the bonding of silica particles into a solid, coherent, and more ordered structure. These processes require energy and are typically driven by elevated temperature and/or pressure. In the case of the spicules studied here, however, such conditions were likely of limited importance, as the specimens were never deeply buried. Another similar process that can be involved is Ostwald ripening, a process, during which larger particles grow at the expense of smaller particles, thus reducing general surface energy (Iler, 1979)

Nevertheless, silica sintering *in vivo,* i.e., at ambient temperature, has been proposed for sponge spicule formation as a result of the catalytic properties of silicatein present within the spicules (Müller *et al*., 2011). Experimental work by Fuchs *et al*. (2014) demonstrated that such catalytic effects can facilitate the transformation of opal-A in sponge

spicules into cristobalite at relatively low temperatures (~859 °C). Given that spicules are biocomposites containing silicatein, this may help to explain how similar phase transformations could proceed over long timescales without the need for high pressure and/or temperature.

The first evidence of this type of transformation is the preservation of the original structure of the spicules, observed in most of the studied specimens. But a crucial line of evidence for distinguishing between these pathways is the occurrence of microspherical silica bodies within spicule-associated pore spaces. The presence of nearly perfect, isolated spheres embedded in nanogranular matrix is difficult to reconcile with a model, involving direct precipitation from solution into open cavities. Under such conditions, nucleation would be expected to occur preferentially on the pore walls, where interfacial energy is minimized, followed by inward growth producing coatings or concentric infill structures. The formation of centrally positioned spheres would require highly improbable conditions, including perfectly symmetric diffusion fields and the sustained suspension of a growing nucleus within the pore fluid.

In contrast, these features are readily explained by solid-state transformation within a silica precursor. In this model, a less ordered silica phase undergoes localized densification and structural reorganization, leading to the formation of a more ordered, lower-water-content phase, expressed as a compact spherical body. This process is inherently associated with volume reduction due to dewatering and densification. As a result, the newly formed sphere contracts relative to the surrounding matrix, producing a gap between the sphere and the pore wall. The presence of such gaps constitutes strong evidence for an *in situ* transformation mechanism, as it reflects a density contrast between the precursor material and the resulting phase. In a dissolution-reprecipitation scenario, externally supplied silica would instead tend to fill available space rather than generate voids.

The spherical morphology arises naturally from isotropic contraction and/or growth within a homogeneous matrix, rather than from isotropic free growth in fluid. The apparent central positioning of the spheres is therefore best interpreted as a geometric consequence of uniform growth and shrinkage within a previously continuous matrix, rather than as a result of nucleation in suspension. In some cases, the microspheres are very regular in shape (Fig. 4B–C), while in other samples they may be elongated and irregular (Fig. 5E–H). This can be explained by the fact that in a more homogeneous environment (matrix), growth is isotropic, producing nearly perfect spheres. In contrast, when the matrix is less homogeneous, growth becomes anisotropic, with certain directions being preferred, resulting in less regular shapes such as elongated spheres and hemispheres. This mechanism eliminates the need for long-distance silica transport and is fully consistent with closed-system behaviour, in which material redistribution occurs locally during phase transformation.

Textural evidence, supporting this interpretation, in the fossil record includes the preservation of the original shape and microstructure, the absence of features, indicative of dissolution or reprecipitation (such as secondary porosity, cements, or truncation surfaces), and a progressive increase in silica density and crystallinity. These features are observed in the sponge spicules studied here. The only porosity present in the Eocene spicules can be attributed to silica dehydration, without removal of material, and is therefore consistent with a closed-system process.

Processes, such as dewatering and diffusion operating without an intermediate dissolution phase, have traditionally been dismissed as mechanisms of diagenetic reorganization, largely because they are considered extremely slow under low-temperature and low-pressure conditions, i.e., in the absence of deep burial. However, this argument becomes less compelling, when considered on a geological timescale. The sponge spicules studied here range in age from approximately 35 to 150 Ma, providing ample time for even slow solid-state processes to proceed. Thus, the preservation of original microstructures, formation of microspheres, coupled with evidence of densification and increased crystallinity, is fully consistent with a solid-state transformation mechanism occurring in a closed system over millions of years.

In the case of the silica modifications, observed in the sponge spicules described here, solid-state transformation appears to have been the dominant process. This interpretation is supported by the preservation of many structural (though not all) and most surface features. Furthermore, occurrences of silica microspheres, embedded within a nanogranular matrix identified as opal-CT, as well as mixtures of spheres and glassy (smooth silica) regions, representing opal-A (as observed in Eocene spicules), and incipient quartz crystals, growing in one direction and composed of nanogranular silica, growing at the expense of the granular matrix (in Jurassic spicules), cannot be adequately explained by a dissolution–reprecipitation mechanism. Instead, these features consistently point to the *in-situ* transformation of silica phases.

This process likely began with the nucleation of low-tridymite within an amorphous matrix (Liesegang *et al*., 2018). It is analogous to the *in vivo* solid-state transition of amorphous calcium carbonate (ACC) to crystalline forms through dehydration (Addadi *et al*., 2003; Du and Amstad, 2020), with silica dehydration acting as the primary driving mechanism in a closed system.

Spicules that underwent this type of diagenesis (characterised by the presence of traces of the original structure and/or microspheres, embedded in a nanogranular matrix, or incipient quartz crystals, composed of nanogranules) provide the best potential for preservation of the original isotopic signal; therefore, only such material should be targeted for isotopic analysis. However, this must be verified by detailed isotopic comparisons of spicules, showing different diagenetic modifications, but originating from the same sample (preferably the same sponge). This is particularly important, given that some recent studies (Slagter *et al*., 2025; Stamm *et al*., 2025) concluded that even slight diagenetic changes can modify the original isotopic composition.

The conclusion of Slagter *et al.* (2025) is based on experimental work, conducted in an open system, where dissolution and reprecipitation operated – consistent with the above discussion of alternative diagenetic pathways. The case of Stamm *et al.* (2025), who analyzed fossil Cretaceous spicules, is different. They reported that spicules of the same

age, but at different stages of diagenetic advancement, differ in isotopic composition by 0.3‰ δ^{30}Si on average. This difference would be understandable, if the dissolution-reprecipitation model applied, as assumed by Stamm *et al.* (2025), but without structural studies of their spicules. On the basis of their observations, we argue that the spicules they analysed underwent a similar diagenesis to that of the Eocene spicules of the present study – namely, solid-state transformation, not dissolution reprecipitation – which should have preserved more or less the original isotopic composition of silica.

For now, several explanations of δ^{30}Si difference between the samples, other than diagenetic alteration, remain possible, making the Stamm *et al*. (2025) argumentation not very strong. First, the spicules examined by Stamm *et al.* (2025) were classified solely by morphology, not taxonomy, meaning they may have come from different sponge taxa that fractionate silicon isotopes differently. More importantly, the reported isotopic difference is not statistically significant: a two-sample Welch's *t*-test yielded $p = 0.34$ (calculated from Stamm *et al.,* 2025, tab. S8), indicating that the difference between the two samples is not statistically meaningful. Additionally, this mean value difference is small, when compared with the natural variability of δ^{30}Si values in spicules from a single extant sponge, which can reach 1.0‰ δ^{30}Si or more (Pisera, unpublished data). Therefore, this issue requires further integrated diagenetic, structural, and isotopic studies. However, the conclusion by Stamm *et al*. (2025) that the diagenetic differences they observed modify the Si isotopic signal is unfounded.

SUMMARY AND CONCLUSIONS

1. All studied Recent sponge spicules are composed of opal-A, with no mineralogical differences among taxa. Their mineral parameters (peak position, d-spacing, FWHM) differ slightly from sinter opal-A.
2. Most Eocene spicules from Australia and Ukraine are preserved as opal-A. Narrower FWHM values in fossil opal-A, compared to those in Recent spicules, indicate incipient diagenesis, even in the absence of visible structural changes under SEM. This suggests that original opal-A can persist in siliceous spicules for approximately 40 million years, provided they have not been subjected to significant temperature or pressure.
3. The structure of the Eocene iridescent spicules from Australia, with fissured outer layers and spongy interiors, likely results from brief, high-temperature exposure during bushfires.
4. The Late Cretaceous spicules are preserved as opal-CT and/or quartz. Opal-CT forms microspheres and hemispheres similar to the Eocene spicules, while quartz spicules show massive internal silica units, made of nanogranules.
5. Most Late Jurassic spicules are preserved as quartz, though some contain opal-CT, indicated by aligned nanogranules and XRD. The dense outer rim of silica nanogranules with relic layering may also be opal-CT. Traces of moganite were also found.
6. Different mineral phases (opal-A, opal-CT, or quartz) can be observed, not only in spicules from the same sample or of the same age, but even within a single spicule. This indicates that silica maturation occurs primarily at the microscale. The presence of euhedral low-cristobalite in some Jurassic spicules reflects later diagenetic overprinting. Structural modification of spicules depends largely on age and locality, with taxonomy playing a smaller role. Hexactinellid spicules tend to preserve internal structures more poorly than those of demosponges, likely due to original differences in skeletal architecture.
7. Early opal-A diagenesis in spicules involves growth of silica microspheres or hemispheres in a nanogranular matrix, marking the transition to opal-CT. The white or opaque appearance of the spicules results from light refraction, caused by silica inhomogeneity, produced during maturation via solid-state transformation, without intermediate mould formation due to dissolution.
8. In the Early Cretaceous and the Late Jurassic spicules, silica microspheres are replaced by dense silica nanogranule blocks. In later diagenesis, euhedral nano- and microquartz crystals form near the surface, likely through fusion or transformation of silica nanogranules.
9. Most micro- and nanoquartz observed in the Jurassic spicules is diagenetic, forming from pre-existing silica nanogranules, rather than direct precipitation. It consists of silica nanogranules and early quartz crystals with diffuse crystalline faces.
10. All the examined spicules, ranging from opal-A to quartz compositions, retain traces of their original structure and morphological details. Diagenesis did not proceed from the external surface toward the centre; rather, it was concentrated in the interior (the main body of the spicule), while the outer layer is the best preserved. In the early stages of diagenesis, the formation of silica microspheres within a similar nanogranular matrix is characteristic and consistent with solid-state transformation processes, without the involvement of dissolution and void formation. In the Jurassic samples, the growth of incipient microquartz follows from the fusion of granular silica, rather than from the precipitation of microquartz crystals. These structural observations suggest that the dominant transformation of silica occurred through solid-state maturation (via dehydration and sintering) and/or Ostwald ripening, rather than by dissolution and re-precipitation from external fluids. Early stages of this process could be added by organics that are part of the spicule biosilica.
11. As a result, fossil spicules, showing preservation similar to that described in this study – i.e., traces of original structure, microspheres, embedded in a nanogranular matrix, and/or incipient microquartz showing fused nanogranular silica – are considered the preferred targets for silicon isotope analysis, in contrast to those modified by dissolution-reprecipitation diagenesis. However, the assumption that such

spicules retain their original isotopic signal must always be verified through carefully integrated structural and isotopic investigations.

12. Our observations should be taken into account when interpreting the diagenetic pathways of fossil spiculites and spicule-rich rocks, such as spiculites and Cretaceous opokas.

CRediT authorship contribution statement:

Andrzej Pisera – Conceptualization, methodology, investigations, interpretations, writing – original draft and review and editing, funding acquisition;

Sylvie Masse and Mohamed Selmane – investigations, reading and editing;

Magdalena Łukowiak – investigation, writing – review and editing.

Declaration of no competing interest:

The authors declare that they have no known competing financial interests or personal relationships that could have appeared to influence the work, reported in this paper.

Acknowledgments

This study was supported by the NCN Grant No. 2016/21/B/ST10/02332 to AP. XRD measurements were performed by G. Kaproń (Faculty of Geology, Warsaw University), who delivered raw numerical data used thereafter for mineralogical analyses (displaying of XRD diffractograms and their interpretation and comparison). We are deeply indebted to two anonymous reviewers for their careful reading of the manuscript and their insightful critiques, which have significantly contributed to its improvement, even though we do not necessarily agree with all of their comments and suggestions.

REFERENCES

Addadi, L, Raz, S. & Weiner, S., 2003. Taking advantage of disorder: amorphous calcium carbonate and its roles in biomineralization. *Advanced Materials,* 15: 959–970.

Arasuna, A., Kigawa, M., Fujii, S., Endo, T., Takahashi, K. & Okuno, M., 2018. Structural characterization of the body frame and spicules of a glass sponge. *Minerals*, 8: 88.

Bertolino, M., Cattaneo-Vietti, R., Pansini, M., Santini, C. & Bavestrello, G., 2017. Siliceous sponge spicule dissolution: In field experimental evidences from temperate and tropical waters. *Estuarine, Coastal and Shelf Science*, 184: 46–53.

Cady, S. L., Wenk, H.-R. & Downing, K. H., 1996. HRTEM of microcrystalline opal in chert and porcelanite from the Monterey Formation, California. *American Mineralogist*, 81: 1380–1395.

Calvert, S. E., 1974. Deposition and diagenesis of silica in marine sediments. In: Hsü, K. J. & Jenkyns, H. C. (eds), *Pelagic Sediments: On Land and under the Sea*. *International Association of Sedimentologists, Special Publication*, 1: 273–299.

Calvert, S. E., 1977. Mineralogy of silica phases in deep-sea cherts and porcelanites. *Philosophical Transactions of the Royal Society of London. Series A, Mathematical and Physical Sciences*, 286: 239–252.

Campbell, K. A., Sannazzaro, K., Rodgers, K. A., Herdianita, N. R. & Browne, P. R. L., 2001. Sedimentary facies and mineralogy of the Late Pleistocene Umukuri silica sinter, Taupo Volcanic Zone, New Zealand. *Journal of Sedimentary Research*, 71: 727–746.

DeBano, L. F., Neary, D. G. & Folliott, P. F., 1998. *Fire's Effects on Ecosystems*. John Wiley & Sons, New York, 352 pp.

De La Rocha, C. L., 2003. Silicon isotope fractionation by marine sponges and the reconstruction of the silicon isotope composition of ancient deep water. *Geology*, 31: 423.

Demaster, D., 2005. The diagenesis of biogenic silica: chemical transformations occurring in the water column, seabed, and crust. *Treatise on Geochemistry*, 7: 87–98.

Du, H. & Amstadt, E., 2020. Water: how does it influence the $CaCO_3$ formation? *Angewandte Chemie, International Edition*, 59: 1798–1816.

Dudik, O., Amorim, S., Xavier, J. R., Rapp, H. T., Silva, T. H., Pires, R. A. & Reis, R. L., 2021. Bioactivity of biosilica obtained from North Atlantic deep-sea sponges. *Frontiers in Marine Science*, 8: 637810.

Ehrlich, H., Demadis, K. D., Pokrovsky, O. S. & Koutsoukos, P. G., 2010. Modern views on desilicification: biosilica and abiotic silica dissolution in natural and artificial environments. *Chemical Reviews*, 110: 4656–89.

Ehrlich, H., Janussen, D., Simon, P., Bazhenov, V. V., Shapkin, N. P., Erler, Ch., Mertig, M., Born, R., Heinemann, S., Hanke, T., Worch, H. & Vournakis, J. N., 2008. Nanostructural organization of naturally occurring composites – Part II: Silica-chitin-based biocomposites. *Journal of Nanomaterials*, 2008: 670235.

Ehrlich, H., Luczak, M., Ziganshin, R., Mikšík, I., Wysokowski, M., Simon, P., Baranowska-Bosiacka, I., Kupnicka, P., Ereskovsky, A., Galli, R., Dyshlovoy, S., Fischer, J., Tabachnick, K. R., Petrenko, J., Jesionowski, T., Lubkowska, A., Figlerowicz, M., Ivanenko, V. N. & Summers, A. P., 2022. Arrested in glass: Actin within sophisticated architectures of biosilica in sponges. *Advanced Science*, 9: 2105059.

Ehrlich, H. & Worch, H., 2007. Sponges as natural composites: from biomimetic potential to development of new biomaterial. In: Custódio, M. R., Lobo-Hajdu, G., Hajdu, E. & Muricy, G. (eds), *Porifera Research: Biodiversity, Innovation and Sustainability.* Museu Nacional, Rio de Janeiro, pp. 217–223.

Elzea, J. M., Odom, I. E. & Miles, W. J., 1994. Distinguishing well-ordered opal-CT and opal-C from high temperature cristobalite by x-ray diffraction. *Analytica Chimica Acta*, 286: 107–116.

Elzea, J. M. & Rice, S. B., 1996. TEM and X-ray diffraction evidence for cristobalite and tridymite stacking sequences in opal. *Clays and Clay Minerals*, 44: 492–500.

Flörke, O. W., Graetsch, H., Martin, B., Röller, K. & Wirth, R., 1991. Nomenclature of micro- and non-crystalline silica minerals, based on structure and microstructure. *Neues Jahrbuch für Mineralogie Abhandlungen. Abhandlungen*, 163: 19–42.

Fontorbe, G., Frings, P. J., De La Rocha, C. L., Hendry, K. R., Carstensen, J. & Conley, D. J., 2017. Enrichment of dissolved silica in the deep equatorial Pacific during the Eocene-Oligocene. *Paleoceanography*, 32: 848–863.

Fontorbe, G., Frings, P. J., De La Rocha, C. L., Hendry, K. R. & Conley, D., 2016. A silicon depleted North Atlantic since the

Palaeogene: evidence from sponge and radiolarian silicon isotopes. *Earth and Planetary Science Letters*, 453: 67–77.

Frings, P. J., Clymans, W., Fontorbe, G., Christina, L. & Conley, D. J., 2016. The continental Si cycle and its impact on the ocean Si isotope budget. *Chemical Geology*, 425: 12–36.

Frisone, V., Pisera, A., Hajdu, E., Preto, N., Zorzi, F. & Zorzin, R., 2014. Isolated spicules of Demospongiae from Mt. Duello (Eocene, Lesssini Mts, norethern Italy): preservation, taxonomy and depositional environment. *Facies*, 60: 883–904.

Fröhlich, F., 2020. The opal-CT nanostructure. *Journal of Non-Crystalline Solids*, 533: 119938.

Fuchs, I., Aluma, Y., Ilan, M. & Mastai, Y., 2014. Induced crystallization of amorphous biosilica to cristobalite by silicatein. *The Journal of Physical Chemistry B*, 118: 2104–2111.

Gammon, P. R. & James, N. P., 2003. Paleoenvironmental controls on upper Eocene biosiliceous neritic sediments, southern Australia. *Journal of Sedimentary Research*, 73: 57–972.

Gammon, P. R., James, N. P. & Pisera, A., 2000. Eocene spiculites and spongolites in southwestern Australia: not deep, not polar, but shallow and warm. *Geology*, 28: 855–858.

Ghisoli, C., Caucia, F. & Marinoni, L., 2010. XRPD patterns of opals: A brief review and new results from recent studies. *Powder Diffraction*, 25: 274–282.

Görlich, S., Samuel, S. J., Best, R. J., Seidel, R., Vacelet, J., Leonarski, F. K., Tomizaki, T., Rellinghaus, B., Pohle, D. & Zlotnikov, I., 2020. Natural hybrid silica/protein superstructure at atomic resolution. *PNAS*, 117, 49: 31088–31093.

Graetsch, H., 1994. Structural characteristics of opaline and microcrystalline silica minerals. In: Heaney, P. J., Prewitt, C. T. & Gibbs, G. V. (eds), *Silica. Physical Behavior, Geochemistry and Materials Applications Review in Mineralogy*, 29: 209–232.

Graetsch, H., Flörke, O. W. & Miehe, G., 1987. Structural Defects in Microcrystalline Silica. *Physics and Chemistry of Minerals*, 14: 249–257.

Guthrie, G. D., Bish, D. L. & Reynolds, R. C., 1995. Modelling the X-ray diffraction pattern of opal-CT. *American Mineralogist*, 80: 869–872.

Hendry, K. R., Georg, R. B., Rickaby, R. E. M., Robinson, L. F. & Halliday, A. N., 2010. Deep ocean nutrients during the Last Glacial maximum deduced from sponge silicon isotopic compositions. *Earth and Planetary Science Letters*, 292: 290–300.

Hendry, K. R. & Robinson, L. F., 2012. The relationship between silicon isotope fractionation in sponges and silicic acid concentration: Modern and core-top studies of biogenic opal. *Geochimica et Cosmochimica Acta*, 81: 1–12.

Herdianita, N. R., Browne, P. R. L., Rodgers, K. A. & Campbell, K. A., 2000a. Mineralogical and textural changes accompanying ageing of silica sinter. *Mineralium Deposita*, 35: 48–62.

Herdianita, N. R., Rogers, K. A. & Browne, P. R. L., 2000b. Routine procedures to characterise the mineralogy of modern and ancient silica sinter deposits. *Geothermics*, 29: 367–375.

Hesse, R., 1989. Silica diagenesis: origin of inorganic and replacement cherts. *Earth-Science Reviews*, 26: 253–284.

Hooper, J. N. A. & Van Soest, R. W. M. (eds), 2002. *Systema Porifera. A Guide to the Classification of Sponges*. Kluwer Academic/Plenum Press, New York, 1708 pp.

Iler, R. K., 1979. *The Chemistry of Silica*. John Wiley & Sons, New York, 866 pp.

Ilieva, A., Mihailova, B., Tsintsov, Z. & Petrov, O., 2007. Structural state of microcrystalline opals: A Raman spectroscopic study. *American Mineralogist*, 92: 1325–1333.

Jones, B., 2021. Siliceous sinters in thermal spring systems: Review of their mineralogy, diagenesis, and fabrics. *Sedimentary Geology*, 413: 105820.

Jones, B. & Renaut, R. W., 2007. Microstructural changes accompanying the opal-A to opal-CT transition: new evidence from the siliceous sinters of Geysir, Haukadalur, Iceland. *Sedimentology*, 54: 921–948.

Jones, J. B. & Segnit, I. R., 1971. The nature of opal. I. Nomenclature and constituent phases. *Journal of the Geological Society of Australia*, 18: 57–68.

Jurkowska, A. & Świerczewska-Gładysz, E., 2020. Evolution of Late Cretaceous Si cycling reflected in formation of siliceous nodules (flints and cherts). *Global and Planetary Change*, 195: 103–334.

Jurkowska, A., Świerczewska-Gładysz, E. & Filipowicz, S., 2026. The role of siliceous sponges in pre-Eocene marine Si cycle as a Si source – a case study from a carbonate environment. *Lethaia,* 59: 1–17.

Kang, S. J. L., 2004. *Sintering: Densification, Grain Growth and Microstructure*. Elsevier, Amsterdam, 265 pp.

Kastner, M., Keene, J. & Gieskes, J., 1977. Diagenesis of siliceous oozes 1. Chemical controls on rate of opal-A to opal-CT transformation - experimental study. *Geochimica et Cosmochimica Acta*, 41: 1041–1051.

Kochman, A. & Matyszkiewicz, J., 2023. The development and origin of the two-stage silicification of Upper Jurassic limestones from the northern part of the Kraków-Częstochowa Upland (Southern Poland). *Geology, Geophysics and Environment*, 49: 225–243.

Lagneau-Hérenger, L., 1962. Contribution à l'étude des spongiaires siliceux du Crétacé inférieur. *Mémoire de la Société Géologique de France, Nouvelle Série*, 41: 1–252.

Lee, D. R., 2007. *Characterization and the Diagenetic Transformation of Non- and Microcrystalline Silica Minerals*. Master's thesis. University of Liverpool, United Kingdom, 20 pp.

Liesegang, M. & Milke, R., 2014. Australian sedimentary opal-A and its associated minerals: Implications for natural silica sphere formation. *American Mineralogist*, 99: 1488–1499.

Liesegang, M., Milke, R. & Berthold, C., 2018. Amorphous silica maturation in chemically weathered clastic sediments. *Sedimentary Geology*, 365: 54–61.

Łukowiak, M., 2015. Late Eocene siliceous sponge fauna of southern Australia: reconstruction based on loose spicules record. *Zootaxa*, 3917: 1–65.

Łukowiak, M., 2016. Fossil and modern sponge fauna of southern Australia and adjacent regions compared: interpretation, evolutionary and biogeographic significance of the late Eocene 'soft' sponges. *Contributions to Zoology*, 85(1): 13–35.

Łukowiak, M., 2020. Utilizing sponge spicules in taxonomic, ecological and environmental reconstructions: a review. *PeerJ*, 8: e10601. https://doi.org/10.7717/peerj.10601

Łukowiak, M. & Pisera, A., 2017. Bodily preserved Eocene non-lithistid demosponge fauna from southern Australia: taxonomy and affinities. *Journal of Systematic Palaeontology*, 15: 473–497.

Łukowiak, M., Pisera, A., Stefanska, T. & Stefanskyi, V., 2022a. High diversity of siliceous sponges in Western Tethyan areas during the Eocene: palaeobiogeographical, ecological and taxonomic significance. *Papers in Palaeontology*, 8: e1416,

Łukowiak, M., Van Soest, R., Klautau, M., Pérez, T., Pisera, A. & Tabachnick, K., 2022b. The terminology of sponge spicules. *Journal of Morphology*, 283: 1517–1545.

Lynne, B.Y. & Campbell, K. A., 2003. Diagenetic transformations (opal-A to quartz) of low- and mid-temperature microbial textures in siliceous hot-spring deposits, Taupo Volcanic Zone, New Zealand. *Canadian Journal of Earth Sciences*, 40: 1679–1696.

Lynne, B. Y. & Campbell, K. A., 2004. Morphologic and mineralogic transitions from opal-A to opal CT in low-temperature siliceous sinter diagenesis, Taupo Volcanic Zone, New Zealand. *Journal of Sedimentary Research*, 74: 561–579.

Lynne, B. Y., Campbell, K. A., James, B. J., Browne, P. R. L. & Moore, J., 2007. Tracking crystallinity in siliceous hot-spring deposits. *American Journal of Science*, 307: 612–641.

Lynne, B. Y., Campbell, K. A., Moore, J. N. & Browne, P. R. L., 2005. Diagenesis of 1900-year-old siliceous sinter (opal-A to quartz) at Opal Mound Roosevelt Hot Springs, Utah, USA. *Sedimentary Geology*, 179: 249–278.

Lynne, B. Y., Campbell, K. A., Moore, J. & Browne, P. R. L., 2008. Origin and evolution of the Steamboat Springs siliceous sinter deposit, Nevada, U.S.A. *Sedimentary Geology*, 210: 111–131.

Maldonado, M., Carmona, M. C., Velásquez, Z., Puig, A., Cruzado, A., López, A. & Young, C. M., 2005. Siliceous sponges as a silicon sink: An overlooked aspect of benthopelagic coupling in the marine silicon cycle. *Limnology and Oceanography*, 50: 799–809.

Maldonado, M., Lopez-Acosta, M., Abalde, S., Martos, I., Ehrlich, H. & Leynaert, A., 2022. On the dissolution of sponge silica: Assessing variability and biogeochemical implications. *Frontiers in Marine Science*, 9: 1005068.

Masse, S., Pisera, A., Laurent, G. & Thibaud, C., 2016. A solid state NMR investigation of recent marine siliceous sponge spicules. *Minerals*, 6: 21.

Matyja, B. A., 2006. Stop A17 – Zalas Quarry - Callovian transgressive to condensed pelagic deposits, Lower to lowermost Middle Oxfordian deposits of sponge megafacies (Figs A63C, A71). In: Wierzbowski, A., Aubrecy, R., Golonka, J., Gutowski, J., Krobicki, M., Matyja, B. A., Pieńkowski, G. & Uchman, A. (eds), *Jurassic of Poland and adjacent Slovakian Carpathians. Field-trip guidebook of 7th International Congress on the Jurassic System. Poland, Kraków, September 6–18, 2006*. Państwowy Instytut Geologiczny, Warszawa, pp. 70–72.

Matyja, B. A., Dembicz, K. & Praszkier, T., 2006. Stop B1.8 – Wrzosowa Quarry, condense Callovian and Lower Oxfordian ammonite succession. In: Wierzbowski, A., Aubrecy, R., Golonka, J., Gutowski, J., Krobicki, M., Matyja, B. A., Pieńkowski, G. & Uchman, A. (eds), *Jurassic of Poland and adjacent Slovakian Carpathians. Field-trip guidebook of 7th International Congress on the Jurassic System. Poland, Kraków, September 6–18, 2006*. Państwowy Instytut Geologiczny, Warszawa, pp . 158–159.

Matyja, B. A. & Tarkowski, R., 1981. Lower and Middle Oxfordian ammonite biostratigraphy at Zalas in the Cracow Upland. *Acta Geologica Polonica*, 31: 1–14.

Matysik, M., Stemmerik, L., Olaussen, S. & Brunstad, H., 2018. Diagenesis of spiculites and carbonates in a Permian temperate ramp succession – Tempelfjorden Group, Spitsbergen, Arctic Norway. *Sedimentology*, 65: 745–774.

Matysik, M., Stemmerik, L., Olaussen, S., Remmel, N., Gianotten, I. P. & Brunstadt, H., 2021. Cherts, spiculites, and collapse breccias – Porosity generation in upper Permian reservoir rocks, Gohta discovery, Loppa High, south-western Barents Sea. *Marine and Petroleum Geology*, 128: 105043.

Mizutani, S., 1977. Progressive ordering of cristobalites silica in the early stage of diagenesis. *Contributions to Mineralogy and Petrology*, 61: 129–140.

Murata, K. J. & Nakata, J. K., 1974. Cristobalitic stage in the diagenesis of diatomaceous shale. *Science*, 184: 567–568.

Müller, W. E., Boreiko, A., Wang, X., Belikov, S. I., Wiens, M., Grebenjuk, V. A., Schloßmacher, U. & Schröder, H. C., 2007. Silicateins, the major biosilica forming enzymes present in demosponges: protein analysis and phylogenetic relationship. *Gene*, 395: 62–71.

Müller, W. E., Wang, X., Chen, A, Hu., S, Gan, L., Schröder, H. C, Schloßmacher, U. & Wiens, M., 2011. The unique invention of the siliceous sponges: their enzymatically made bio-silica skeleton. In: Müller, W. (ed), *Molecular Biomineralization. Progress in Molecular and Subcellular Biology*, 52: 251–281.

Müller, W. E. G., Wang, X., Kropf, K., Ushijima, H., Geurtsen, W., Eckert, C., Tahir, M. N., Tremel, W., Boreiko, A., Schloßmacher, U., Li, J. & Schröder, H. C., 2008. Bioorganic/inorganic hybrid composition of sponge spicules: matrix of the giant spicules and of the comitalia of the deep sea Hexactinellid *Monorhaphis*. *Journal of Structural Biology*, 161: 188–203.

Pisera, A., 2003. Some aspects of silica deposition in lithistid demosponge desmas. *Microscopy Research and Technique*, 62: 312–326.

Pisera, A., Bitner, M. A. & Fromont, J., 2023. Eocene phymaraphiniid demosponges from South Western Australia: filling the gap. *Acta Palaeontologica Polonica*, 68: 261–272.

Pisera, A., Łukowiak, M., Masse, S., Tabachnick, K., Fromont, J., Ehrlich, H. & Bertolino, M., 2021. Insights into the structure and morphogenesis of the giant basal spicule of the glass sponge *Monorhaphis chuni*. *Frontiers in Zoology*, 18: 58.

Rodgers, K. A., Browne, P. R. L., Buddle, T. F., Cook, K. L., Greatrex, R. A., Hampton, W. A., Herdianita, N. R., Holland, G. R., Lynne, B. Y., Martin, R., Newton, Z., Pastars, D., Sannazarro, K. L. & Teece, C. I. A., 2004. Silica phases in sinters and residues from geothermal fields of New Zealand. *Earth Science Reviews*, 66: 1–61.

Rodgers, K. A. & Cressey, G., 2001. The occurrence, detection and significance of moganite (SiO_2) among some silica sinters. *Mineralogical Magazine*, 65: 157–167.

Roisnel, T., Rodríquez-Carvajal, J., 2001. WinPLOTR: a Windows tool for powder diffraction pattern analysis, *Material Science Forum,* 378–381: 118–123.

Sandford, F., 2003. Physical and chemical analysis of the siliceous skeletons in six sponges of two groups (Demospongiae and Hexactinellida). *Microscopy Research and Technique*, 62: 336–355.

Schrammen, A., 1910–1912. Die Kieselspongien der oberen Kreide von Nordwest-Deutschland. I. Teil, Tetraxonia, Monaxonia

und Silicea incertae sedis. Teil 2. Triaxonia (Hexactinellida), *Palaeontographica, Suppl*., 5: 1–385.

Schröder, H. C., Natalio, F., Shukoor, I., Tremel, W., Schloßmacher, U., Wang, X. H. & Müller, W. E. G., 2007. Apposition of silica lamellae during growth of spicules in the demosponge *Suberites domuncula*: biological/biochemical studies and chemical/biomimetical confirmation. *Journal of Structural Biology*, 159: 325–334.

Schwab, D. W. & Shore, R. E., 1971. Mechanism of internal stratification of siliceous sponge spicules. *Nature*, 232: 501–502.

Shimizu, K., Nishi, M., Sakate, Y., Kawanami, H., Bito, T., Arima, J., Leria, L. & Maldonado, M., 2024. Silica-associated proteins from hexactinellid sponges support an alternative evolutionary scenario for biomineralization in Porifera. *Nature Communications*, 15: 181.

Sitarz, M., Wyszomirski, P., Handke, B. & Jeleń, P., 2014. Moganite in selected Polish chert samples: the evidence from MIR, Raman and X-ray studies. *Spectrochimica Acta. Part A, Molecular and biomolecular spectroscopy,* 122: 55–58.

Slagter, S., Wang, J., Syverson, D. D., Asael, D., Planavsky, N. J. & Tarhan, L. G., 2025. Silicon isotopic exchange in silica minerals. *Geochimica et Cosmochimica Acta* 405: 1–14.

Stamm, F. M., Pickering, R. A., Frings, P. J., Frick, D. A., Richoz, S. & Conley, D. J., 2025. Impact of diagenesis on biogenic silica- structural, chemical, and isotope proxies. *Journal of Geophysical Research: Biogeosciences*, 130: e2024JG008160.

Trammer, J., 1982. Lower to Middle Oxfordian sponges of the Polish Jura. *Acta Geologica Polonica*, 32: 1–39.

Trammer, J., 1989. Middle to Upper Oxfordian sponges of the Polish Jura. *Acta Geologica Polonica*, 39: 49–91.

Tréguer, P. J., Sutton, J. N., Brzezinski, M., Charette, M. A., Devries, T., Dutkiewicz, S., Ehlert, C., Hawkings, J., Leynaert, A., Liu, S. M., Llopis Monferrer, N., López-Acosta, M., Maldonado, M., Rahman, S., Ran, L. & Rouxel, O., 2021. Reviews and syntheses: The biogeochemical cycle of silicon in the modern ocean. *Biogeosciences*, 18: 1269–1289.

Uriz, M.-J., 2006. Mineral skeletogenesis in sponges. *Canadian Journal of Zoology*, 84: 322–356.

Uriz, M.-J., Turon, X. & Becerro, M., 2000. Silica deposition in demosponges: spiculogenesis in *Crambe crambe*. *Cell and Tissue Research*, 301: 299–309.

Uriz, M.-J., Turon, X., Becerro, M. & Agell, G., 2003. Siliceous spicules and skeleton frameworks in sponges: origin, diversity, ultrastructural patterns, and biological functions. *Microscopy Research and Technique*, 62: 279–99.

Voronkina, A., Cárdenas, P., Adam, J., Meissner, H., Nowacki, K., Joseph, Y., Tabachnick, K. R. & Ehrlich, H., 2025. Biosilica 3D micromorphology of Geodiidae sponge spicules is patterned by F-actin. *Microscopy Research and Technique*, 88: 1701–1711.

Wang, X., Schloßmacher, U., Jochum, K. P., Gan, L., Stoll, B., Uriz, I. & Müller, W. E. G., 2010. Silica-protein composite layers of the giant basal spicules from Monorhaphis: basis for their mechanical stability. *Pure and Applied Chemistry*, 82: 175–192.

Weaver, J. C. & Morse, D. E., 2003. Molecular biology of demosponge axial filaments and their roles in biosilicification. *Microscopy Research and Technique*, 62: 356–367.

Weaver, J. C., Pietrasanta, L. I., Hedin, N., Chmelka, B. F., Hansma, P. K. & Morse, D. E., 2003. Nanostructural features of demosponge biosilica. *Journal of Structural Biology*, 144: 271–281.

Wiese, F., Reich, M. & Schlüter, N., 2013. The marine late Cretaceous (Campanian) from the Hannover area. In: Reitner, J. & Reich, M. (eds), *Palaeobiology and Geobiology of Fossil Lagerstätten through Earth History. A Joint Conference of the "Paläontologische Gesellschaft" and the "Palaeontological Society of China"*, *Göttingen, Germany, September 23–27, 2013. Field Guide to Excursions.* Geoscience Museum of the Georg-August University, Göttingen, pp. 45–51.

Wille, M., Sutton, J., Ellwood, M. J., Sambridge, M., Maher, W., Eggins, S. & Kelly, M., 2010. Silicon isotopic fractionation in marine sponges: A new model for understanding silicon isotopic variations in sponges. *Earth and Planetary Science Letters*, 292: 281–289.

Williams, L. A. & Crerar, D. A., 1985. Silica diagenesis. II. General mechanisms. *Journal of Sedimentary Petrology*, 55: 312–321.

Williams, L. A., Parks, G. A. & Crerar, D. A., 1985. Silica diagenesis I. Solubility controls. *Journal of Sedimentary Petrology*, 55: 301–311.

Wilson, M. J., 2014. The structure of opal-CT revisited. *Journal of Non-crystalline Solids*, 405: 68–75.

Wise, S. W. & de Weaver, F. M., 1974. Chertification of oceanic sediments. In: Hsü, K. J. & Jenkyns, H. C. (eds), *Pelagic Sediments: On Land and under the Sea. Special Publication of the International Association of Sedimentologists*, 1: 301–326.

Woesch, A., Weaver, J. C., Kazanci, M., Dauphin, Y., Aizenberg, J., Morse, D. E. & Fratzl, P., 2006. Micromechanical properties of biological silica in skeletons of deep-sea sponges. *Journal of Material Research*, 21: 2068–2078.

Xue, S.-H., Xie, H., Ping, H., Li, Q.-C., Su, B. L. & Fu, Z.-Y., 2015. Induced transformation of amorphous silica to cristobalite on bacterial surfaces. *RSC Advances*, 88: 71844–71848.